Published in final edited form as:

Neuron. 2018 April 18; 98(2): 366–379.e4. doi:10.1016/j.neuron.2018.03.024.

Reciprocal circuits linking the prefrontal cortex with dorsal and ventral thalamic nuclei

David P. Collins[1], **Paul G. Anastasiades**[1], **Joseph J. Marlin**, and **Adam G. Carter**[*]

Center for Neural Science, New York University, 4 Washington Place, New York, NY 10003

SUMMARY

Reciprocal interactions between the prefrontal cortex (PFC) and thalamus play a critical role in cognition, but the underlying circuits remain poorly understood. Here we use optogenetics to dissect the specificity and dynamics of cortico-thalamo-cortical networks in the mouse brain. We find that cortico-thalamic (CT) neurons in prelimbic PFC project to both mediodorsal (MD) and ventromedial (VM) thalamus, where layer 5 and 6 inputs activate thalamo-cortical (TC) neurons with distinct temporal profiles. We show that TC neurons in MD and VM in turn make distinct connections in PFC, with MD preferentially and strongly activating layer 2/3 cortico-cortical (CC) neurons. Finally, we assess local connections from superficial CC to deep CT neurons, which link thalamo-cortical and cortico-thalamic networks within the PFC. Together our findings indicate that PFC strongly drives neurons in the thalamus, whereas MD and VM indirectly influence reciprocally connected neurons in the PFC, providing a mechanistic understanding of these circuits.

eTOC BLURB

Collins, Anastasiades et al., (2018) show that prefrontal cortex (PFC) engages multiple thalamic nuclei. Dorsal and ventral thalamus in turn target distinct networks within the PFC. Finally, local connectivity in the PFC completes a loop connecting thalamic input with cortico-thalamic output.

INTRODUCTION

The prefrontal cortex (PFC) plays a central role in cognition (Euston et al., 2012; Miller and Cohen, 2001), and is disrupted in neuropsychiatric disorders (Egan and Weinberger, 1997). The rodent PFC communicates directly with several higher-order thalamic nuclei, including the mediodorsal (MD) and ventromedial (VM) thalamus (Gabbott et al., 2005; Krettek and

[*]Corresponding Author & Lead Contact: adam.carter@nyu.edu.

[1]These authors contributed equally

DECLARATION OF INTERESTS

The authors have no financial conflicts of interest.

AUTHOR CONTRIBUTIONS

Conceptualization, A.G.C., D.P.C., J.M.M. and P.G.A.; Investigation, D.P.C., J.M.M. and P.G.A.; Writing – Original Draft, A.G.C., D.P.C. and P.G.A.; Writing – Review & Editing, A.G.C., D.P.C. and P.G.A.; Supervision, A.G.C.; Funding Acquisition, A.G.C.

Price, 1977), which are also engaged in goal-directed behaviors (Guo et al., 2017; Parnaudeau et al., 2013). Recent studies highlight an important role for these long-range networks in maintaining reverberant activity within the PFC and other parts of frontal cortex (Bolkan et al., 2017; Guo et al., 2017; Schmitt et al., 2017). However, little is known about the synaptic organization of the underlying circuits, or the dynamics that support ongoing communication between PFC and thalamus.

Inputs to first-order sensory thalamus are often divided into feed-forward “driver” and feed-back “modulator” pathways (Sherman, 2016). Driver inputs stemming from ascending sensory pathways are strong but exhibit short-term depression (Castro-Alamancos, 2002; Chen and Regehr, 2003). In contrast, modulator inputs arising from layer 6 (L6) cortico-thalamic (CT) neurons are weak but show marked facilitation (Alexander et al., 2006; Cruikshank et al., 2010; Reichova and Sherman, 2004). Higher-order thalamic nuclei like MD and VM lack direct sensory input, and instead may receive driver input from layer 5 (L5) CT neurons (Li et al., 2003; Sherman, 2016). However, while PFC inputs to thalamus play a key role in sustaining persistent activity during behavior (Schmitt et al., 2017), the relative influence of L5 and L6 CT neurons remains unexplored.

Thalamic inputs to cortex can also be divided into feed-forward “first-order” and feed-back “higher-order” pathways (Sherman, 2016). In sensory cortex, first-order inputs densely innervate layer 4 (L4) to drive activity in the local network (Agmon and Connors, 1991; LeVay and Gilbert, 1976), whereas higher-order inputs target superficial layer 1 (L1) (Castro-Alamancos and Connors, 1997; Jones, 2001). In contrast, the PFC lacks a traditional thalamo-recipient layer (Van De Werd et al., 2010), with both MD and VM axons targeting superficial layers (Deniau et al., 1994; Groenewegen, 1988). MD inputs to PFC are usually thought to activate the local network (Pirot et al., 1994; Uylings et al., 2003), but recent work suggests a modulatory role (Schmitt et al., 2017). VM inputs to the PFC are less explored, but engage a variety of superficial neurons (Cruikshank et al., 2012).

While thalamic input primarily arrives in superficial layers of cortex, CT output arises from deep layers (Harris and Shepherd, 2015). To understand how thalamus and PFC generate sustained activity, it is critical to uncover how these inputs and outputs are connected. One possibility is that thalamic inputs drive cortico-cortical (CC) neurons, which indirectly relay activity to deep layer CT neurons. While this arrangement occurs in other cortices (Crandall et al., 2017; Yamawaki and Shepherd, 2015), thalamic input to the PFC may also directly contact CT neurons to form a direct reciprocal connection (Kuroda et al., 1993; White and Hersch, 1982). Moreover, thalamic inputs can evoke robust feed-forward inhibition in the cortex, which could regulate activity of local and long-range networks (Cruikshank et al., 2007; Gabernet et al., 2005; Isaacson and Scanziani, 2011). Understanding how MD and VM inputs influence different cell types in the PFC is needed to determine the properties of thalamo-cortical loops important for cognitive processing.

Here we combine anatomical tracing, targeted recordings, and a variety of optogenetic techniques to assess both long-range and local circuits that link the PFC and thalamus. We first show that individual CT axons can bifurcate to both MD and VM, where L5 and L6 inputs differentially engage reciprocally-connected thalamo-cortical (TC) neurons. We then

determine how MD and VM influence distinct populations of projection neurons across multiple layers of PFC. Finally, we show how intra-cortical connections from superficial CC to deep CT neurons link thalamo-cortical input with cortico-thalamic output. Together, our findings highlight the cell-type and input-specific local and long-range circuits that are responsible for linking PFC with multiple higher-order thalamic nuclei.

RESULTS

PFC activates reciprocally connected neurons in MD and VM

To identify the higher-order nuclei that mediate long-range reciprocal connections between PFC and thalamus, we co-injected AAV-DIO-ChR2-YFP and red retrobeads into the PFC of adult Emx1-Cre mice (Fig. 1A). This approach restricted viral expression to the cortex and prevented retrograde infection of the thalamus, which often occurred in wild-type mice with pan-neuronal viruses, regardless of the viral serotype (*data not shown*). PFC axons overlapped with retrogradely labeled thalamo-cortical (TC) neurons in both mediodorsal (MD) and ventromedial (VM) thalamus (Fig. 1B; n = 6 mice), with similar numbers of labeled cells in each nucleus (Fig. S1). Consistent with previous studies (Kuramoto et al., 2017; Vertes, 2001), PFC axons and TC neurons were predominantly found in the lateral aspect of MD along its rostro-caudal extent, with no apparent spatial segregation observed in VM (Fig. S1). These results provide an anatomical substrate for reciprocal feed-back loops linking the PFC with the thalamus.

To study the properties of cortico-thalamic connections, we combined optogenetics with targeted whole-cell recordings from retrogradely labeled TC neurons (Fig. S2). Optogenetic stimulation of PFC inputs in the presence of TTX and 4-AP (Little and Carter, 2013; Petreanu et al., 2009) evoked robust monosynaptic excitatory postsynaptic currents (EPSCs) in both MD (n = 7 cells, 4 mice) and VM (n = 7 cells, 4 mice), which were blocked by the AMPA receptor antagonist NBQX (10 μM; n = 3 cells each, 3 mice each) (Fig. S2). In sensory thalamus, cortico-thalamic synapses often facilitate (Alexander et al., 2006; Cruikshank et al., 2010), which could sustain activity between PFC and thalamus. During repetitive stimulation in the absence of TTX and 4-AP, we found that PFC-evoked EPSCs were also strongly facilitating, with similar paired-pulse ratio (PPR) in MD and VM (Fig. 1C & S2; PPR = $EPSC_5/EPSC_1$: MD = 3.6 ± 0.4, n = 13 cells, 10 mice; VM = 3.0 ± 0.4, n = 12 cells, 6 mice; p = 0.13).

We next asked whether PFC inputs are sufficiently strong to drive action potential (AP) firing of TC neurons. Current-clamp recordings indicated that cells in MD and VM have similar subthreshold and suprathreshold physiology (Fig. S2). PFC inputs evoked bursts of APs from resting membrane potential (RMP), but only single APs from −55 mV (Fig. S2; MD: n = 7 cells, 4 mice, VM: n = 7 cells, 6 mice), consistent with two distinct modes of firing in TC neurons (Llinás and Jahnsen, 1982). To study facilitating PFC inputs, we delivered trains of 10 Hz stimulation at an intensity that was initially subthreshold. At RMP, TC neurons fired bursts of APs on the second or third pulse and were subsequently silent (Fig. 1D & S2; MD: n = 7 cells, 4 mice, VM: n = 7 cells, 5 mice). At −55 mV, firing progressively increased across the train, reliably following input without decrement (Fig. 1E & S2), with faster latency to the first AP (Fig. S2). These findings indicate that PFC inputs

evoke AP firing at both MD and VM TC neurons via direct, monosynaptic connections. They also highlight how the resting state of TC neurons dynamically regulates synaptic responses and evoked firing.

L5 and L6 CT neurons send diverging projections to thalamus

PFC input to MD and VM displayed remarkably similar synaptic properties, suggesting they may originate from a single population of dual-projecting pyramidal neurons. To test this hypothesis, we next co-injected red and green cholera toxin subunit B (CTB) into the ipsilateral MD and VM (Fig. 2A; n = 3 mice). After allowing for retrograde transport, we observed MD-projecting cortico-thalamic (CT) neurons in the PFC, and VM-projecting CT neurons in both PFC and adjacent motor cortex (Fig. S3). Most PFC CT neurons were located in layer (L6), with a second, smaller population also present in layer 5 (L5) (Fig. 2B; L5 = 26 ± 0.1%, L6 = 74 ± 0.1%). Interestingly, CT neurons in both layers were often co-labeled (dual-labeled cells; L5 = 36 ± 10%, L6 = 42 ± 5%), indicating that individual pyramidal neurons can make diverging projections to MD and VM (Fig. 2C & S3).

To further confirm that CT neurons can project to both nuclei, we injected canine adenovirus expressing Cre recombinase (CAV2-Cre) into either MD (n = 3 mice) or VM (n = 3 mice) (Fig. 2D). After allowing for retrograde transfection, we injected Cre-dependent AAV-DIO-YFP into the ipsilateral PFC to label CT neurons, along with red retrobeads to label PFC-projecting TC neurons. We observed dense axon labeling in both MD and VM, confirming that CT neurons can project to both thalamic nuclei (Fig. 2E). Dual labeling of thalamic nuclei was also observed using AAVretro-Cre instead of CAV2-Cre (Tervo et al., 2016), although in this case CT neurons were restricted to L5, with minimal labeling in L6 (Fig. S3; n = 6 mice). To confirm that injections did not leak across nuclei, we co-injected CTB to visualize the injection site (Fig. S3). As a second line of evidence we performed the AAVretro-Cre experiments in Ai14 reporter mice, with pronounced retrogradely labeled neurons in motor cortex following injection in VM but not MD (Fig. S3; n = 6 mice). Retrogradely labeled CT axons were also observed projecting via the pyramidal tract to other midbrain and pontine structures, but not to contralateral PFC or basolateral amygdala (Fig. 2F). These findings demonstrate that both L5 and L6 CT neurons can send diverging axonal projections to both MD and VM.

L5 CT inputs depress and activate TC neurons only temporarily

The presence of CT neurons in multiple layers of PFC is consistent with two distinct output streams to the thalamus, with L5 CT neurons providing feed-forward “driver” inputs that could strongly activate TC neurons (Sherman, 2016). To isolate L5 CT inputs, we took advantage of the fact that they overlap with pyramidal tract (PT) neurons, whereas L6 CT neurons do not (Harris and Shepherd, 2015). To confirm the suitability of this strategy, we injected AAVretro-Cre into the pons, followed by Cre-dependent AAV-DIO-ChR2-YFP into the ipsilateral PFC to label PT neurons, along with red CTB into the ipsilateral MD to label CT neurons (Fig. 3A; n = 3 mice). We observed strong overlap of PT and CT neurons in superficial L5, which was absent from L6 (Fig. 3B; CT overlap: superficial L5 = 80 ± 3%, deep L5 = 8 ± 1%, L6 = 0.6 ± 0.8%). We next used this approach to study connectivity and dynamics of L5 CT inputs onto TC neurons in both MD and VM. In contrast to our findings

for the total PFC input to thalamus, we found that during repetitive stimulation, L5 CT-evoked EPSCs strongly depressed at both nuclei, with PPR decreasing during trains (Fig. 3C & S3; PPR = $EPSC_5/EPSC_1$: MD = 0.3 ± 0.2; VM = 0.5 ± 0.2; p = 0.24; n = 6 cells each, 3 mice). In current-clamp recordings, L5 CT inputs evoked either an initial burst at RMP, or a single AP at −55 mV, with firing restricted to the start of trains and unable to follow sustained activity (Fig. 3D,E & S3; MD: n = 4 cells, 4 mice VM: n = 4 cells, 4 mice). These findings indicate parallel PFC outputs to MD and VM, with L5 CT depressing and L6 CT facilitating.

MD and VM inputs preferentially target L5 over L6 CT neurons

Our findings indicate that PFC can strongly activate reciprocally connected TC neurons located in both MD and VM. We next examined if equivalent connectivity exists in the reverse direction, with thalamic inputs targeting CT neurons in PFC. To identify thalamic inputs, we injected AAV-SynaptoTag into the ipsilateral MD or VM, which labels axons red and synapses green (Xu and Südhof, 2013). Consistent with established anatomy (Krettek and Price, 1977), we found MD axons were densest in deep L1 and L3, whereas VM axons were concentrated in more superficial L1 (Fig. 4A; n = 3 mice each). However, both MD and VM axons and synapses were also present in deep layers, suggesting they may contact a variety of cell types distributed across multiple layers the PFC (Fig. 4B).

To study thalamo-cortical circuitry, we co-injected AAV-ChR2 into one thalamic nucleus, and retrobeads into both nuclei. After allowing for expression and transport, we performed targeted recordings from retrogradely labeled L5 (450–550 μm from pial surface) and L6 (650–850 μm from pial surface) CT neurons (Fig. 4C). We found L5 CT neurons have larger dendrites than L6 neurons and distinct physiology (Fig. 4C & S4), but observed no differences between MD-, VM- and dual-projecting cells (Fig. S4). To study monosynaptic responses and prevent recurrent activity, we recorded synaptic responses from pairs of L5 and L6 CT neurons in the presence of TTX and 4-AP. Thalamus-evoked EPSCs were larger at L5 CT neurons, for both MD (Fig. 4D; L5 vs. L6 = 143 ± 22 pA vs. 24 ± 6 pA, $p < 0.0001$, n = 17 pairs, 11 mice) and VM (Fig. 4E; L5 vs. L6 = 126 ± 12 pA vs. 26 ± 11 pA, $p < 0.0001$, n = 18 pairs, 11 mice). We quantified this bias as the EPSC amplitude ratio for each pair (L6/L5 amplitude ratio), observing similar ratios for both inputs (Fig. 4F & S5; MD = 0.09, CI: 0.04 – 0.23, p = 0.003; VM = 0.04, CI: 0.01 – 0.13, $p < 0.0001$). These results determine that both MD and VM make monosynaptic connections onto L5 CT neurons in the PFC, but largely avoid L6 CT neurons, which constitute the main population that provides cortical output to thalamus.

MD inputs are strongly biased onto L5 CC over L5 CT neurons

While thalamic inputs contact CT neurons, their primary target could be another population of pyramidal neurons. The PFC also contains cortico-cortical (CC) neurons that project to contralateral PFC and are distributed over multiple layers (Anastasiades et al., 2018a; Dembrow et al., 2010). Recordings from retrogradely labeled CC and CT neurons in L5 confirmed that the physiological properties of these cells are distinct (Fig. S4 & S6). Furthermore, morphological reconstructions from two-photon images indicated that L5 CC neurons have more compact apical dendrites, which could limit their ability to sample

superficial thalamic inputs (Fig. 5A). To compare thalamic inputs at L5 CC and CT neurons, we recorded optogenetically evoked responses at neighboring pairs of retrogradely labeled cells in the presence of TTX and 4-AP. Surprisingly, we found that MD-evoked EPSCs were much stronger at L5 CC neurons (Fig. 5B; CC = 310 ± 51 pA, CT = 106 ± 24 pA, $p < 0.0001$, n = 10 pairs, 6 mice). In contrast, VM-evoked EPSCs showed no such bias (Fig. 5C; CC = 177 ± 33 pA, CT = 197 ± 34 pA, $p = 0.6$, n = 12 pairs, 6 mice). These differences were again highlighted in the CC/CT amplitude ratio, which was 2.92 (CI: 1.84 – 4.62, $p = 0.002$) for MD and 0.94 (CI: 0.45 – 1.95, $p = 0.62$) for VM (Fig. 5D). These findings indicate that MD input is biased onto CC neurons over CT neurons in L5, whereas VM input is equivalent at both populations, suggesting different functions for these inputs.

In addition to differences in EPSC amplitude at the two L5 cell types, we noted that EPSC decays were significantly slower at L5 CT neurons (Fig. 5D & S5). One explanation for these prolonged kinetics is targeting to more distal dendrites at these cells (Marlin and Carter, 2014; Spruston et al., 1994). To study subcellular targeting, we activated thalamic inputs at discrete locations across the dendritic arbor (Fig. 5E) (Anastasiades et al., 2018a; Petreanu et al., 2009). In L5 CC neurons, we found that both MD and VM inputs peaked at the soma and became progressively smaller in the dendrites. In contrast, in L5 CT neurons, both inputs peaked at the apical dendrites, indicating that they selectively target this domain. These differences in targeting were highlighted by comparing the normalized distributions of EPSCs across the somato-dendritic axis (Fig. 5F; MD: $p = 0.0003$, n = 8 CC neurons, 7 CT neurons, 11 mice; VM: $p = 0.0001$, n = 7 CC neurons, 8 CT neurons, 6 mice). These findings highlight how MD and VM inputs primarily target the soma and proximal dendrites of L5 CC neurons, but the distal apical dendrites of L5 CT neurons.

MD inputs preferentially activate L2/3 over L5 CC neurons

CC neurons are also found in superficial layers, which receive prominent input from both MD and VM (Cruikshank et al., 2012; Little and Carter, 2012). We next assessed any cross-laminar bias of MD and VM inputs by recording at pairs of retrogradely labeled L2/3 (200–350 μm from pial surface) and L5 CC neurons from the same slice in the presence of TTX and 4-AP (Fig. 6A). We found that MD-evoked EPSCs were much larger at L2/3 CC neurons, indicating that they target superficial layers (Fig. 6B; L2/3 = 467 ± 91 pA, L5 = 153 ± 30 pA, $p = 0.0006$, n = 11 pairs, 5 mice). In contrast, VM-evoked EPSCs were similar at L2/3 and L5 CC neurons, showing no strong bias between these cell types (Fig. 6C; L2/3 = 146 ± 33 pA, L5 = 115 ± 20 pA, $p = 0.7$, n = 10 pairs, 5 mice). The presence and absence of layer-specific targeting was reflected in the L2/3 to L5 amplitude ratios, which were biased for MD (2.95, CI: 1.48 – 5.88, $p = 0.01$), but close to unity for VM (1.09, CI: 0.75 – 1.58, $p = 0.56$) (Fig. 6D). Interestingly, comparing EPSC amplitudes at L2/3 CC neurons indicated that the strength of MD input was much greater than for VM (Fig. 6B & C). Plotting EPSC amplitude against LED intensity ruled out an effect of stimulation strength, suggesting that MD, but not VM, may provide strong driver input to PFC (Fig. 6D). Finally, thalamic inputs may also target L6 CC neurons (Crandall et al., 2017), but we found that neither MD nor VM inputs evoked sizeable EPSCs at L6 CC neurons when using stimulation parameters that evoked responses in superficial layers (Fig. S5). These findings

show that thalamic inputs are prominent in superficial layers, with MD inputs strongest at L2/3 CC neurons.

We next asked whether thalamic inputs drive AP firing in PFC, or perhaps have a more modulatory influence on local activity (Schmitt et al., 2017). In current-clamp, we found that MD inputs robustly drive AP firing of L2/3 CC neurons but yielded only subthreshold EPSPs at L5 CC neurons (Fig. 6E & F; $p < 0.0001$, n = 7 pairs, 3 mice). In contrast, VM inputs were unable to drive either L2/3 or L5 CC neurons, instead evoking subthreshold EPSPs followed by a brief hyperpolarization, possibly reflecting feed-forward inhibition (Fig. 6E, n = 8 pairs, 3 mice). The absence of VM-evoked AP firing again occurred despite the higher light intensities used in these recordings (Fig. 6F). The ability of MD inputs to evoke elevated EPSC amplitudes and AP firing across separate experiments and despite lower light intensities argues against a systematic experimental bias in ChR2 expression. These findings support a role for MD in driving L2/3 CC neurons, with VM providing broader, more modulatory influence across a variety of cell types and cortical layers.

MD and VM inputs show distinct short-term dynamics in the PFC

Differences in evoked firing between MD and VM could be explained by relative strength of direct excitation (E) or feed-forward inhibition (I). To examine differences in E/I balance at L2/3 CC neurons, we recorded EPSCs at −70 mV and IPSCs at the excitation reversal potential (E_{rev}). We found that both MD and VM evoked EPSCs and IPSCs (Fig. 7A), with comparable E/I ratios for inputs from the two nuclei (Fig. 7B; MD = 0.72, CI: 0.57–0.89, n = 11 cells, 5 mice; VM = 0.51, CI: 0.31–0.85, n = 10 cells, 4 mice; p = 0.13). However, we consistently observed larger EPSCs and IPSCs in response to MD stimulation (Fig. 7B), indicating that differences in evoked inhibition are unlikely to explain distinct firing responses.

Having established that both MD and VM inputs trigger excitation and inhibition at L2/3 CC neurons, we next examined responses to repetitive activity. In sensory cortex, first-order thalamic inputs often exhibit pronounced depression (Beierlein and Connors, 2002; Stratford et al., 1996), whereas higher-order thalamic input in some cases facilitate (Castro-Alamancos and Connors, 1997; Cruikshank et al., 2012). We found that MD-evoked EPSCs depressed during 10 Hz stimulation trains, with progressively decreasing PPR (Fig. 7C,D & S7; PPR = $EPSC_5/EPSC_1 = 0.70 \pm 0.05$; n = 11 cells, 5 mice). In contrast, VM-evoked EPSCs initially facilitated, and remained elevated during trains (Fig. 7C,D & S7; PPR = $EPSC_5/EPSC_1 = 0.92 \pm 0.06$; n = 11 cells, 4 mice). These results indicate different short-term dynamics of these connections, reminiscent of first- and higher-order inputs to sensory cortex.

In contrast to excitation, we found that both MD- and VM-evoked IPSCs strongly depressed during repetitive activity (Fig. 7C & D; PPR = $IPSC_5/IPSC_1$ = MD: 0.13 ± 0.04; VM: 0.21 ± 0.03; p = 0.77). This depressing inhibition suggested a growing E/I imbalance that could enable sustained cortical activation (Isaacson and Scanziani, 2011). However, in current-clamp recordings we found that MD inputs readily evoked AP firing at the start of stimulation trains, but ultimately became subthreshold (Fig. 7E & F; n = 7 cells, 3 mice). In contrast, VM inputs failed to evoke AP firing at any point during trains, eliciting only

subthreshold EPSPs (Fig. 7E & F; n = 6 cells, 3 mice). These results indicate that MD and VM inputs exhibit distinct short-term plasticity and have different influences on the PFC.

L2/3 CC neurons contact L5 CT neurons in the local circuit

While thalamo-cortical inputs preferentially activate L2/3 CC neurons, cortico-thalamic outputs arise from CT neurons in deep layers of PFC. We next asked whether CC neurons can target L5 or L6 CT neurons to complete the feed-back loop that is important for reverberant activity (Bolkan et al., 2017; Guo et al., 2017; Schmitt et al., 2017). We injected AAVretro-Cre and CTB into the contralateral PFC, along with retrobeads into the ipsilateral MD, and Cre-dependent AAV-dflox-ChR2 in the ipsilateral PFC (Fig. 8A). To study local connectivity, we then recorded optogenetically-evoked EPSCs from triplets of L5 CT, L6 CT and ChR2-negative L5 CC neurons in the presence of TTX and 4-AP. We found that CC-evoked EPSCs were strongest onto L5 CT neurons, with smaller responses at neighboring L5 CC neurons, and negligible responses at L6 CT neurons (Fig. 8B & C; n = 7 triplets, 3 mice), indicating that the local network contacts cortico-thalamic output pathways.

While these results show that CC neurons contact CT neurons, they do not reveal in which layer presynaptic CC neurons are located. To study local connectivity, we used Cre-dependent, soma-targeted optogenetics, in which a mutated version of the fast opsin Chronos is tagged with the C-terminal domain of Kv2.1 (st-ChroME) (Baker et al., 2016; Klapoetke et al., 2014; Mardinly et al., *in press*), restricting expression to the soma and proximal dendrites (Fig. 8D). This approach eliminates light-evoked responses at the axon and distal dendrites, allowing us to directly correlate the site of light stimulation with the somatic location of presynaptic neurons. To confirm restricted activation, we first recorded from st-ChroME+ L2/3 and L5 CC neurons while stimulating at multiple locations along the X and Y axes (Fig. 8E & S8), showing a lateral resolution of 50 μm, with APs restricted to L2/3 or L5 (Fig. 8F & S8). We then used this approach to produce layer-specific input maps, assessing connections from st-ChroME+ L2/3 and L5 CC neurons onto L5 CT neurons (Fig. 8G). Light-evoked CC-EPSCs were time-locked and reliable across trials (Fig. 8H & S8), due to the rapid spike latency achieved by st-ChroME activation (Fig. S8; L2/3 vs. L5: 2.3 ± 0.05 ms vs. 2.2 ± 0.13 ms; p = 0.22; n = 6 pairs, 3 mice). We found that CC-EPSCs could be readily evoked when illuminating over L2/3 and L5 (Fig. 8H & S8), and after correcting for differences in presynaptic firing (Fig. S8; Bureau et al., 2004), we observed prominent CC input from both layers (Fig. 8I; L2/3 = 43 ± 4%, L5 = 36 ± 4%; n = 16 CT cells, 4 mice). Together, these findings indicate that the L2/3 CC neurons activated by thalamic inputs can in turn contact L5 CT neurons that project to thalamus, closing the loop between these two brain regions.

DISCUSSION

Our findings define the cellular and synaptic properties of reciprocal circuits between the PFC and thalamus. Cortico-thalamic pathways are mediated by L5 and L6 CT neurons, which send branching projections to MD and VM, and differentially drive AP firing of TC neurons. Thalamo-cortical pathways are similarly divided into two projections, with MD strongly activating L2/3 CC neurons in PFC, and VM influencing multiple layers. Their

distinct targeting, combined with different dynamics during ongoing activity, indicate these pathways have unique functions. Finally, although thalamo-cortical inputs do not directly activate CT neurons, preferential local connectivity from L2/3 CC to L5 CT neurons functions as an intermediary between thalamo-cortical and cortico-thalamic networks.

Our findings illustrate how two populations of CT neurons in PFC communicate with TC neurons in two distinct higher-order thalamic nuclei. Cortical inputs to the thalamus are often functionally segregated based on their layer of origin (Bickford, 2015). L5 CT inputs are “drivers” that have high release probability and reliably drive AP firing of TC neurons (Sherman, 2016). Consistent with this idea, L5 CT inputs from PFC to MD and VM evoke firing at the start of stimulus trains via depressing synapses. In contrast, L6 CT inputs are “modulators” that have low initial release probability and weaker effects on firing (Sherman and Guillery, 1998). However, because these cells are more numerous, they may also have robust influence on TC neurons, particularly during repetitive activity. In agreement with this idea, the overall PFC input to MD and VM evokes robust firing via strongly facilitating synapses. These results suggest L6 CT neurons may play an underappreciated role in helping to sustain persistent activity of higher-order thalamus during behavior.

Several of our experiments indicate that individual CT neurons send diverging projections to both MD and VM. These branching PFC outputs may synchronize AP firing of TC neurons across multiple thalamic nuclei. However, it is important to remember that cortico-thalamic excitation does not exist in isolation, as L6 CT inputs also innervate the thalamic reticular nucleus (TRN) to evoke feed-forward inhibition in thalamic relay nuclei (Cruikshank et al., 2010; Olsen et al., 2012). Interactions between PFC and TRN are proposed to play an important role in shaping thalamic activity during attentional tasks (Halassa and Acsady, 2016; Wimmer et al., 2015). Ultimately, dynamic shifts in cortically-evoked excitation and feed-forward inhibition will influence how PFC activates TC neurons (Crandall et al., 2015), and thus gates its own thalamic input via these reciprocal circuits.

Higher-order thalamic nuclei are often envisioned to relay information between cortical regions (Sherman, 2016; Theyel et al., 2010). While recent studies have focused on direct thalamo-cortical loops (Bolkan et al., 2017; Guo et al., 2017; Schmitt et al., 2017), or direct cortico-cortical pathways (Guo et al., 2014; Mao et al., 2011; Suter and Shepherd, 2015; Zagha et al., 2013), indirect cortico-thalamo-cortical relays may also be important (Saalmann, 2014; Saalmann et al., 2012). PFC provides input across the rostral-caudal and ventral-medial axes of VM, with similar distributions observed after injections in motor cortex (Guo et al., 2017), suggesting that a reciprocal di-synaptic pathway may functionally link these regions. In the future, it will be interesting to determine the relative importance of PFC signaling via thalamo-cortical, cortico-cortical and cortico-thalamo-cortical loops.

Our results also show how MD and VM differentially contact and influence a range of projection neurons in the PFC. Thalamic inputs to sensory cortices are segregated anatomically, with first-order thalamic inputs enriched in L4 (Douglas and Martin, 2004) and higher-order thalamic inputs enriched in L1 (Castro-Alamancos and Connors, 1997). These inputs also play distinct roles, with the former relaying sensory information, and the latter mixed sensory-motor feed-back (Roth et al., 2016; Sherman, 2016). The function of

thalamic input to PFC and other frontal cortices is less clear, particularly as rodent PFC lacks the traditional thalamo-recipient L4 (Van De Werd et al., 2010), with MD inputs arborizing in deep L1 and L3, and VM inputs primarily enriched in superficial L1. We observe that MD inputs drive AP firing in L2/3 CC neurons in PFC, similar to first-order inputs to L4 of sensory cortex. However, these inputs depress, perhaps suggesting a more supportive role during sustained activity *in vivo* (Schmitt et al., 2017). In contrast, VM provides subthreshold excitation across many layers with facilitating synapses, reminiscent of higher-order inputs to sensory cortex. Thus, despite major differences in anatomy, both sensory and frontal cortices receive two distinct classes of thalamic input, with one directly engaging the local network, and the other providing modulatory input.

Despite these similarities, there are notable differences between frontal and sensory cortices, which may lead to differences in cortico-thalamic processing. In sensory cortex, ascending pathways relay information to L4, where it undergoes local processing before being passed on to superficial layers (Douglas and Martin, 2004; Thomson and Bannister, 2003). In contrast, callosal input from the contralateral hemisphere primarily targets neurons in L2/3 and L5, leading to an initial segregation of thalamic and cortical input (Petreanu et al., 2007; Wise and Jones, 1976). In PFC, both MD and callosal input converge on L2/3 neurons, which also receive input from amygdala and hippocampus (Carter and Little, 2012). Reverberant activity in L2/3 is thought to be essential for delay period activity, suggesting that this convergence may play an important role in sustaining PFC activity (Kritzer and Goldman-Rakic, 1995; Schmitt et al., 2017; Wang et al., 2007; Wang, 2001). In sensory cortex, thalamic inputs can also target neurons in deep layers, with prominent bands of axons in L5 and L6 (Constantinople and Bruno, 2013; Crandall et al., 2017; Gilbert and Wiesel, 1983). In contrast, thalamic axons in deeper layers of PFC are sparse, which may explain the relatively weak thalamic input to L6 neurons.

Both MD and VM display pronounced axon labelling in L1, which allows them to target the apical dendrites of L5 neurons. Dendritic targeting appears specific to L5 CT neurons, and may contribute to neuronal computation in these cells (Spruston, 2008; Takahashi et al., 2016). For example, MD and VM inputs may trigger dendritic Ca^{2+} spikes or shape back-propagating action potentials, despite relatively weak somatic responses (Schiller et al., 1997; Stuart and Häusser, 2001). Interestingly, such dendritic targeting is not observed for other inputs to L5 CT neurons (Anastasiades et al., 2018a). Distal targeting of thalamic input may allow for monosynaptic thalamo-cortical feed-back, while simultaneously avoiding deleterious strong loops between cortex and thalamus (Crick and Koch, 1998). Indeed, avoiding such connectivity appears to be a consistent feature of the cortex, as somatic recordings from other regions also observe thalamic bias onto CC neurons over neighboring CT neurons (Crandall et al., 2017; Yamawaki and Shepherd, 2015).

Our experiments also provide a synaptic link between thalamic activation of L2/3 CC neurons and PFC output by L5 CT neurons. Recent *in vivo* studies highlight an important role for callosal connectivity in maintaining activity in frontal cortex (Li et al., 2016). However, it is also clear that reverberant cortico-thalamic activity can be sustained in the absence of callosal input (Li et al., 2016). Ipsilateral connections between pyramidal neurons may link the site of thalamic input in superficial layers to cortical output in deep layers.

However, local circuitry in PFC has been less explored than in other parts of cortex, where CC neurons are known to contact cortico-fugal neurons (Anderson et al., 2010; Brown and Hestrin, 2009; Morishima and Kawaguchi, 2006). Soma-targeted optogenetics allowed us to demonstrate strong connections from L2/3 and L5 CC neurons onto L5 CT neurons. This arrangement closes an ipsilateral cortico-thalamo-cortical loop, with connections onto L5 CT neurons helping to ensure ongoing driver-like input to thalamus.

In addition to activating excitatory networks, thalamic inputs to PFC evoke pronounced feed-forward inhibition. As observed in sensory cortices, both MD- and VM-evoked inhibition rapidly depressed during sustained synaptic activity (Cruikshank et al., 2007; Cruikshank et al., 2010; Gabernet et al., 2005). Within PFC, MD-evoked inhibition is primarily mediated via parvalbumin-positive interneurons (Delevich et al., 2015), whereas VM inputs can activate a diversity of interneurons in L1 (Cruikshank et al., 2012), including those mediating disinhibition (Lee et al., 2013; Letzkus et al., 2011). Therefore, although VM does not appear to be a strong driver of PFC, it may regulate E/I balance, which plays a key functional role in the cortex (Fu et al., 2014; Letzkus et al., 2015), including within PFC (Kamigaki and Dan, 2017; Pi et al., 2013; Wang et al., 2004). Interestingly, deficits in E/I balance within PFC have also been implicated in many neuropsychiatric disorders (Marin, 2012; Yizhar et al., 2011). Our findings suggest perturbing the local circuit, via too much or too little inhibition, may also disrupt long-range circuits linking PFC and thalamus. Because PFC contacts multiple thalamic nuclei, this will not only impact local activity in PFC, but also cause deficits in downstream cortical regions.

Together, our findings provide mechanistic insights into the organization and dynamics of cortico-thalamic circuits linked to behavior and psychiatric disorders. In the future, it will be important to test the roles of these distinct cell types and connections in both *in vivo* physiology and behavior. In the thalamus, persistent activity during cognitive tasks (Schmitt et al., 2017) could reflect either sparse activation of depressing L5 CT inputs (Groh et al., 2008) or sustained activation of facilitating L6 CT inputs. The diverging projections of L5 and L6 CT neurons predict PFC will drive synchronous activity in MD and VM (Saalmann et al., 2012). In the PFC, MD inputs will preferentially influence L2/3 CC neurons, whose projections across hemispheres may contribute to stabilizing cortical activity during the delay period (Li et al., 2016). In contrast, VM inputs will broadly influence neurons across multiple layers, and may also relay feed-back from motor cortex (Guo et al., 2017). Although our findings indicate MD inputs strongly drive the PFC, subthreshold responses could also combine with other inputs to sustain activity PFC during behavioral tasks (Schmitt et al., 2017). Finally, the connections from L2/3 CC to L5 CT neurons complete an indirect thalamo-cortico-thalamic loop, which may contribute to persistent cortical activity across time (Bolkan et al., 2017; Guo et al., 2017; Schmitt et al., 2017).

STAR METHODS

Contact for Reagent and Resource Sharing

Further information and requests for resources and reagents should be directed to and will be fulfilled by the Lead Contact, Adam Carter (adam.carter@nyu.edu)

Experimental Model and subject details

Acute slices were prepared from healthy, immune-competent P42-P70 (mean ± STDEV = 56.6 ± 6.6) wild-type mice, Ai14 reporter mice (Madisen et al., 2010), and Emx1-Cre mice (Gorski et al., 2002), all bred on a C57 BL/6J background (n = 235 mice total). No animals had been involved in previous procedures. Animals were group-housed with same-sex littermates in a dedicated animal care facility and were on a 12-h light/dark cycle at 18–23°C. Food and water were available ad libitum. All physiology and anatomy experiments used male and female mice, and no significant differences were found between groups. All procedures followed guidelines approved by the New York University animal welfare committee.

Method Details

All experiments were replicated in at least 3 animals. No formal method for randomization was used and experimenters were not blind to experimental groups. No pre-test analyses were used to estimate sample sizes. No data were excluded from final analyses.

Stereotaxic injections—P28-P42 mice were anesthetized with a mixture of ketamine and xylazine and head fixed in a stereotax (Kopf Instruments). A small craniotomy was made over the injection site, through which retrograde tracers and viruses were injected. Injection site coordinates were relative to bregma (mediolateral, dorsoventral, and rostrocaudal axes: PFC = ±0.35, −2.1, +2.2 mm; anterior MD thalamus = −0.4, −3.5, −0.4 mm; anterior VM thalamus = −2.9, −3.4, −0.4 mm, at an angle of 30° from upright), pons = +0.5, −4.7, −4.0 mm. Borosilicate pipettes with 5–10 μm tip diameters were backfilled and 100–500 nl was pressure-injected using a Nanoject II (Drummond) with 30–45 second inter-injection intervals. For retrograde labeling, pipettes were filled with undiluted red or green retrobeads (Lumafluor) or cholera toxin subunit B (CTB) conjugated to Alexa 488 or 647 (Thermo Fisher). AAV-DJ-hSyn-mCherry-IRES-eGFP-syb2 (SynaptoTag; Stanford) was used for non-conditional axon labeling. Optogenetic stimulation was achieved using AAV1-hSyn-hChR2-eYFP, AAV1-EF1a-DIO-hChR2-eYFP, AAV1-EF1a-dflox-hChR2-mCherry (UPenn Vector Core), or AAV expressing soma-tagged ChroME (st-ChroME), which is a variant of Chronos with a M140E point mutation (Mardinly et al., *in press*) (AAV9-CAG-DIO-ChronosM140E-ST-p2A-H2B-mRuby, provided by Hillel Adesnik). In some experiments, simultaneous virus and retrobead injections were mixed in a 2:1 virus:bead ratio. Following injections, the pipette was left in place for an additional 10 min before being slowly withdrawn. Retrograde-Cre experiments were carried out in a similar manner, with injection of either CAV2-Cre (Montpellier) or AAVretro-Cre (pAAV-EF1a-mCherry-IRES-Cre, Addgene), in either wild-type or Ai14 reporter mice. After all injections, animals were returned to their home cages for 2–4 weeks before being used for experiments.

Slice preparation—Mice were anesthetized with an intraperitoneal injection of a lethal dose of ketamine/xylazine and perfused intracardially with an ice-cold cutting solution containing the following (in mM): 65 sucrose, 76 NaCl, 25 $NaHCO_3$, 1.4 NaH_2PO_4, 25 glucose, 2.5 KCl, 7 $MgCl_2$, 0.4 Na-ascorbate, and 2 Na-pyruvate (bubbled with 95% O_2/5% CO_2). 300 μm coronal sections were cut in this solution and transferred to ACSF containing the following (in mM): 120 NaCl, 25 $NaHCO_3$, 1.4 NaH_2PO_4, 21 glucose, 2.5 KCl, 2 $CaCl_2$,

1 $MgCl_2$, 0.4 Na-ascorbate, and 2 Na-pyruvate (bubbled with 95% O_2/5% CO_2). Slices were recovered for 30 min at 35°C and stored for at least 30 min at 24°C. All experiments were conducted at 30–32°C.

Electrophysiology—Targeted whole-cell recordings were made from projection neurons in PFC and thalamus using infrared-differential interference contrast. In the PFC, layers were defined by distance from the pial surface: L2/3: 200–350 μm; L5: 400–550 μm; L6: 650–850 μm. CC and CT neurons were identified by the presence of retrobeads or CTB. To eliminate biases, the color of beads or CTB used to label MD- and VM-projecting neurons was alternated across experiments. For clarity, figures show MD-projecting CT neurons were labeled green and VM-projecting CT neurons labeled red. For recordings from st-ChroME-infected CC neurons, cells in L2/3 or L5 were identified by mRuby expression. In the thalamus, MD and VM were defined visually, and TC neurons identified by the presence of retrobeads or CTB.

For voltage-clamp experiments, borosilicate pipettes (3–5 MΩ) were filled with the following (in mM): 135 Cs-gluconate, 10 HEPES, 10 Na-phosphocreatine, 4 Mg_2-ATP, 0.4 NaGTP, 10 TEA, 2 QX-314, and 10 EGTA, pH 7.3 with CsOH (290–295 mOsm). For current-clamp recordings, borosilicate pipettes (3–5 MΩ) were filled with the following (in mM): 135 K-gluconate, 7 KCl, 10 HEPES, 10 Na-phosphocreatine, 4 Mg_2-ATP, 0.4 NaGTP, and 0.5 EGTA, pH 7.3 with KOH (290–295 mOsm). In some cases, 30 μM Alexa Fluor-594 or -488 (Thermo Fisher) were added to visualize morphology with two-photon microscopy. In all experiments, 10 μM CPP was used to block NMDA receptors. In all voltage-clamp experiments, 1 μM ZD-7288 was included to block HCN channels. In some voltage-clamp experiments, 1 μM TTX was included to block action potentials (APs), along with 0.1 mM 4-AP and 4 mM external Ca^{2+} to restore presynaptic glutamate release. In some experiments, 10 μM NBQX was used to block AMPA receptors, and 10 μM gabazine was used to block $GABA_A$ receptors. All chemicals were from Sigma or Tocris Bioscience.

Physiology data were collected with a Multiclamp 700B amplifier (Axon Instruments) and National Instruments boards using custom software in MATLAB (MathWorks). Signals were sampled at 10 kHz and filtered at either 5 kHz for current-clamp recordings or 2 kHz for voltage-clamp recordings. Series resistance was 10–25 MΩ and not compensated.

Optogenetics—Glutamate release was triggered by activating channelrhodopsin-2 (ChR2) present in presynaptic terminals of either thalamic inputs to the PFC, or PFC inputs to the thalamus, as previously described (Little and Carter, 2012). In the thalamus, MD and VM neurons from the same slice were recorded in alternating order. In the PFC, L5 cells were always recorded first to allow for a standard comparison across layers. LED power was adjusted until responses <1 nA were seen in L5 CT (for L5/L6 CT pairs) or L5 CC (for L5 CC/CT pairs and L5/L6/L2/3 CC sets) neurons, with the same power used for all cells in that slice. ChR2 was activated with 1–8 ms pulses of 473 nm light from a blue light-emitting diode (LED; 473 nm; Thorlabs) through a 10X 0.3 NA objective (Olympus) with a power range of 0.1–20 mW. Subcellular targeting recordings utilized a 60X 1.0 NA objective (Olympus) with an effective illumination diameter <200 μm. For all other recordings in the PFC, the objective was always centered 350 μm from the pial surface of the cortex. Similar

results were also obtained with the LED centered over the cell body (Fig. S5). For recordings in the thalamus, the objective was always centered over the recorded neuron.

Soma-restricted optogenetics—To map the outputs of soma-targeted st-ChroME+ CC neurons, stimulation parameters were developed to produce robust, spatially restricted AP firing of these cells. Recordings were made from sequential pairs of L2/3 and L5 st-ChroME + CC neurons located in the same slice of prelimbic PFC. Blue (473 nm) LED light was focused through a 60X 1.0NA objective (Olympus), with the aperture minimized to provide an effective beam diameter of ~50 μm. With the objective centered at the soma, LED power was adjusted to produce firing in L2/3 st-ChroME+ CC neurons in response to brief (0.25 – 4 ms) light pulses. Using these parameters, similar firing was observed in whole-cell and cell-attached mode, across both L2/3 and L5 (Fig. S8A). For all subsequent experiments, 2 ms LED pulses were used, as this duration consistently evoked firing in L2/3 and L5 neurons across all trials (Fig. S8A). To determine the spatial resolution of this approach, the objective was shifted relative to the soma in both x and y axes, using 50 μm steps. This usually yielded APs restricted to a single stimulation site, consistent with a 50 μm resolution (Fig. 8F & S8C). L5 neurons often fired at multiple stimulation sites along the y-axis, yielding more APs per cell than L2/3 neurons (Fig. S8D). However, all recorded cells retained sub-laminar resolutions (Fig. 8F), allowing for comparison of inputs evoked from individual layers (Anastasiades and Butt, 2012; Anastasiades et al., 2018b)

To account for differences in viral expression across animals and slices (Little and Carter, 2013; Mao et al., 2011), LED power was initially adjusted while recording from a st-ChroME+ CC neuron to provide reliable, spatially restricted firing. Layer 5 CT neurons were then identified by CTB labelling and targeted for voltage-clamp recording as described above. To stimulate st-ChroME+ CC neurons in different layers, the objective was cycled along the y (laminar) axis at 0.1 Hz through L1-5 (0–700 μm, 50 μm resolution). Due to the reliable and rapid onset of firing in st-ChroME+ CC neurons (~2 ms), LED-evoked inputs were time-locked (Fig. 8H), and stable across trials (Fig. S8E). For each CT neuron, raw EPSCs were assigned to individual layers based on stimulation distance from the pia, and individual input maps were peak normalized, producing cross-layer input maps for each cell (Fig. S8F). Finally, to account for differences in excitability at L2/3 and L5 st-ChroME+ CC neurons (Fig. S8D), *post-hoc* scaling was applied to L2/3 input (Bureau et al., 2004).

Two-photon microscopy—Two-photon imaging was performed on a custom microscope, as previously described (Chalifoux and Carter, 2010). Briefly, a Titanium:Sapphire laser (Coherent Ultra II) tuned to 810 nm was used to excite Alexa Fluor-594 or -488 to image dendrite morphology. Imaging was performed with a 60X 1.0NA objective (Olympus). Morphological reconstruction and analysis of two-photon images were conducted in Neurolucida 360 (MBF Bioscience).

Histology—Mice were anesthetized and perfused intracardially with 0.01 M PBS followed by 4% PFA. Brains were stored in 4% PFA for 12–18 hours at 4° C before being washed three times (30 minutes each) in 0.01 M PBS. Slices were cut on a VT-1000S vibratome (Leica) at 70 μm thickness and placed on gel-coated glass slides. ProLong Gold anti-fade reagent with DAPI (Invitrogen) or VectaShield with DAPI (Vector Labs) was applied to the

surface of the slices, which were then covered with a glass coverslip. Fluorescent images were taken on an Olympus VS120 microscope, using a 10X 0.25NA objective (Olympus). For cell counts, images were taken on a Leica TCS SP8 confocal microscope, using a 10X 0.4NA objective (Olympus).

Data analysis—Off-line analysis was performed using Igor Pro (WaveMetrics). For current-clamp recordings, input resistance was measured using the steady-state response to a 500 ms, −50 or −100 pA current injection. The membrane time constant (tau) was measured using exponential fits to these same hyperpolarizations. Voltage sag due to h-current was calculated by taking the minimum voltage in the first 200 ms, subtracting the average voltage over the final 50 ms, and then dividing by the steady-state value. Action potential latencies were measured as the time between LED stimulation and membrane voltage crossing 0 mV. Rebound action potentials in thalamic neurons were counted in the 50 ms following −100 pA current steps. For voltage-clamp recordings, PSC amplitudes were measured as the average value across 1 ms around the peak response.

For co-localization analysis in PFC, cell counting was performed in ImageJ on a multi-color image of retrogradely labeled neurons with DAPI labeling. Labeled cell bodies were manually counted in regions 300 μm × 1000 μm in prelimbic PFC. Distance from the pial surface was used to sort cells into 50 μm bins. The number of cells per bin was averaged across 3 slices from each animal (n = 3 animals), and these average values were used to calculate averages ± SEM. across animals. For cell counting in the thalamus, ROIs for MD and VM were calculated in each slice after aligning to the Allen Brain Atlas at the appropriate rostro-caudal co-ordinate. Axon distributions in PFC and thalamus were quantified using un-binned fluorescence profiles relative to distance from the pia (in PFC) and distance from the midpoint of the MD or VM (in thalamus). The average fluorescence profile for each animal was peak-normalized before calculating a final average ± SEM.

Quantification and Statistical Analysis

N values are reported within the Results and Supplemental Figure legends as number of recorded cells and animals (for physiology) or number of animals (for anatomy). Summary data are reported in the text and figures as arithmetic mean ± SEM. Ratio data displayed in figures on logarithmic axes are reported as geometric mean ± 95% confidence interval (CI). In some graphs with three or more traces, SEM waves are omitted for clarity. Statistical analyses were performed using Prism 7.0 (GraphPad Software). Comparisons between unpaired data were performed using two-tailed Mann-Whitney tests. Comparisons between data recorded in pairs were performed using two-tailed Wilcoxon matched-pairs signed rank tests. Ratio data were log-transformed and compared to a theoretical median of 0 using Wilcoxon signed rank tests. For paired comparisons of more than two groups, Friedman tests with Dunn’s multiple comparisons tests were performed. Comparisons between groups across a range of variables (such as between L2/3 and L5 CC neurons to a range of LED pulse durations) were made using repeated measures two-way ANOVA with Sidak’s multiple comparison test. For all comparisons, no assumptions were made regarding data distributions, and significance was defined as $p < 0.05$.

Supplementary Material

Refer to Web version on PubMed Central for supplementary material.

Acknowledgments

We thank the Carter lab, Chris McBain and Michael Long for helpful discussions and comments on the manuscript. We thank Hillel Adesnik for helping with soma-targeted optogenetics and providing associated reagents. This work was supported by NIH T32 GM007308 (DPC) and NIH R01 MH085974 (AGC).

References

Agmon A, Connors BW. 1991; Thalamocortical responses of mouse somatosensory (barrel) cortex in vitro. Neuroscience. 41:365–379. [PubMed: 1870696]

Alexander GM, Fisher TL, Godwin DW. 2006; Differential response dynamics of corticothalamic glutamatergic synapses in the lateral geniculate nucleus and thalamic reticular nucleus. Neuroscience. 137:367–372. [PubMed: 16360282]

Anastasiades PG, Butt SJ. 2012; A role for silent synapses in the development of the pathway from layer 2/3 to 5 pyramidal cells in the neocortex. J Neurosci. 32:13085–13099. [PubMed: 22993426]

Anastasiades PG, Marlin JJ, Carter AG. 2018a; Cell-Type Specificity of Callosally Evoked Excitation and Feedforward Inhibition in the Prefrontal Cortex. Cell Rep. 22:679–692. [PubMed: 29346766]

Anastasiades PG, Marques-Smith A, Butt SJB. 2018b; Studies of cortical connectivity using optical circuit mapping methods. J Physiol. 596:145–162. [PubMed: 29110301]

Anderson CT, Sheets PL, Kiritani T, Shepherd GM. 2010; Sublayer-specific microcircuits of corticospinal and corticostriatal neurons in motor cortex. Nat Neurosci. 13:739–744. [PubMed: 20436481]

Baker CA, Elyada YM, Parra A, Bolton MM. 2016Cellular resolution circuit mapping with temporal-focused excitation of soma-targeted channelrhodopsin. Elife. :5.

Beierlein M, Connors BW. 2002; Short-term dynamics of thalamocortical and intracortical synapses onto layer 6 neurons in neocortex. J Neurophysiol. 88:1924–1932. [PubMed: 12364518]

Bickford ME. 2015; Thalamic Circuit Diversity: Modulation of the Driver/Modulator Framework. Front Neural Circuits. 9:86. [PubMed: 26793068]

Bolkan SS, Stujenske JM, Parnaudeau S, Spellman TJ, Rauffenbart C, Abbas AI, Harris AZ, Gordon JA, Kellendonk C. 2017; Thalamic projections sustain prefrontal activity during working memory maintenance. Nat Neurosci. 20:987–996. [PubMed: 28481349]

Brown SP, Hestrin S. 2009; Intracortical circuits of pyramidal neurons reflect their long-range axonal targets. Nature. 457:1133–U1189. [PubMed: 19151698]

Bureau I, Shepherd GM, Svoboda K. 2004; Precise development of functional and anatomical columns in the neocortex. Neuron. 42:789–801. [PubMed: 15182718]

Castro-Alamancos MA. 2002; Properties of primary sensory (lemniscal) synapses in the ventrobasal thalamus and the relay of high-frequency sensory inputs. J Neurophysiol. 87:946–953. [PubMed: 11826059]

Castro-Alamancos MA, Connors BW. 1997; Thalamocortical synapses. Prog Neurobiol. 51:581–606. [PubMed: 9175158]

Chalifoux JR, Carter AG. 2010; GABAB receptors modulate NMDA receptor calcium signals in dendritic spines. Neuron. 66:101–113. [PubMed: 20399732]

Chen C, Regehr WG. 2003; Presynaptic modulation of the retinogeniculate synapse. J Neurosci. 23:3130–3135. [PubMed: 12716920]

Constantinople CM, Bruno RM. 2013; Deep cortical layers are activated directly by thalamus. Science. 340:1591–1594. [PubMed: 23812718]

Crandall SR, Cruikshank SJ, Connors BW. 2015; A corticothalamic switch: controlling the thalamus with dynamic synapses. Neuron. 86:768–782. [PubMed: 25913856]

Crandall SR, Patrick SL, Cruikshank SJ, Connors BW. 2017; Infrabarrels Are Layer 6 Circuit Modules in the Barrel Cortex that Link Long-Range Inputs and Outputs. Cell Rep. 21:3065–3078. [PubMed: 29241536]

Crick F, Koch C. 1998; Constraints on cortical and thalamic projections: the no-strong-loops hypothesis. Nature. 391:245–250. [PubMed: 9440687]

Cruikshank SJ, Ahmed OJ, Stevens TR, Patrick SL, Gonzalez AN, Elmaleh M, Connors BW. 2012; Thalamic Control of Layer 1 Circuits in Prefrontal Cortex. J Neurosci. 32:17813–17823. [PubMed: 23223300]

Cruikshank SJ, Lewis TJ, Connors BW. 2007; Synaptic basis for intense thalamocortical activation of feedforward inhibitory cells in neocortex. Nat Neurosci. 10:462–468. [PubMed: 17334362]

Cruikshank SJ, Urabe H, Nurmikko AV, Connors BW. 2010; Pathway-specific feedforward circuits between thalamus and neocortex revealed by selective optical stimulation of axons. Neuron. 65:230–245. [PubMed: 20152129]

Delevich K, Tucciarone J, Huang ZJ, Li B. 2015; The mediodorsal thalamus drives feedforward inhibition in the anterior cingulate cortex via parvalbumin interneurons. J Neurosci. 35:5743–5753. [PubMed: 25855185]

Dembrow NC, Chitwood RA, Johnston D. 2010; Projection-specific neuromodulation of medial prefrontal cortex neurons. J Neurosci. 30:16922–16937. [PubMed: 21159963]

Deniau JM, Menetrey A, Thierry AM. 1994; Indirect nucleus accumbens input to the prefrontal cortex via the substantia nigra pars reticulata: A combined anatomical and electrophysiological study in the rat. Neuroscience. 61:533–545. [PubMed: 7526269]

Douglas RJ, Martin KA. 2004; Neuronal circuits of the neocortex. Annu Rev Neurosci. 27:419–451. [PubMed: 15217339]

Egan MF, Weinberger DR. 1997; Neurobiology of schizophrenia. Curr Opin Neurobiol. 7:701–707. [PubMed: 9384552]

Euston DR, Gruber AJ, McNaughton BL. 2012; The Role of Medial Prefrontal Cortex in Memory and Decision Making. Neuron. 76:1057–1070. [PubMed: 23259943]

Fu Y, Tucciarone JM, Espinosa JS, Sheng N, Darcy DP, Nicoll RA, Huang ZJ, Stryker MP. 2014; A cortical circuit for gain control by behavioral state. Cell. 156:1139–1152. [PubMed: 24630718]

Gabbott PLA, Warner TA, Jays PRL, Salway P, Busby SJ. 2005; Prefrontal cortex in the rat: Projections to subcortical autonomic, motor, and limbic centers. J Comp Neurol. 492:145–177. [PubMed: 16196030]

Gabernet L, Jadhav SP, Feldman DE, Carandini M, Scanziani M. 2005; Somatosensory integration controlled by dynamic thalamocortical feed-forward inhibition. Neuron. 48:315–327. [PubMed: 16242411]

Gilbert CD, Wiesel TN. 1983; Functional organization of the visual cortex. Prog Brain Res. 58:209–218. [PubMed: 6138809]

Gorski JA, Talley T, Qiu M, Puelles L, Rubenstein JLR, Jones KR. 2002; Cortical excitatory neurons and glia, but not GABAergic neurons, are produced in the Emx1-expressing lineage. J Neurosci. 22:6309–6314. [PubMed: 12151506]

Groenewegen HJ. 1988; Organization of the Afferent Connections of the Mediodorsal Thalamic Nucleus in the Rat, Related to the Mediodorsal Prefrontal Topography. Neuroscience. 24:379–431. [PubMed: 2452377]

Groh A, de Kock CP, Wimmer VC, Sakmann B, Kuner T. 2008; Driver or coincidence detector: modal switch of a corticothalamic giant synapse controlled by spontaneous activity and short-term depression. J Neurosci. 28:9652–9663. [PubMed: 18815251]

Guo ZV, Inagaki HK, Daie K, Druckmann S, Gerfen CR, Svoboda K. 2017; Maintenance of persistent activity in a frontal thalamocortical loop. Nature. 545:181–186. [PubMed: 28467817]

Guo ZV, Li N, Huber D, Ophir E, Gutnisky D, Ting JT, Feng G, Svoboda K. 2014; Flow of cortical activity underlying a tactile decision in mice. Neuron. 81:179–194. [PubMed: 24361077]

Halassa MM, Acsady L. 2016; Thalamic Inhibition: Diverse Sources, Diverse Scales. Trends Neurosci. 39:680–693. [PubMed: 27589879]

Harris KD, Shepherd GM. 2015; The neocortical circuit: themes and variations. Nat Neurosci. 18:170–181. [PubMed: 25622573]

Isaacson JS, Scanziani M. 2011; How inhibition shapes cortical activity. Neuron. 72:231–243. [PubMed: 22017986]

Jones EG. 2001; The thalamic matrix and thalamocortical synchrony. Trends Neurosci. 24:595–601. [PubMed: 11576674]

Kamigaki T, Dan Y. 2017; Delay activity of specific prefrontal interneuron subtypes modulates memory-guided behavior. Nat Neurosci. 20:854–863. [PubMed: 28436982]

Klapoetke NC, Murata Y, Kim SS, Pulver SR, Birdsey-Benson A, Cho YK, Morimoto TK, Chuong AS, Carpenter EJ, Tian Z, et al. 2014; Independent optical excitation of distinct neural populations. Nat Methods. 11:338–346. [PubMed: 24509633]

Krettek JE, Price JL. 1977; The cortical projections of the mediodorsal nucleus and adjacent thalamic nuclei in the rat. J Comp Neurol. 171:157–191. [PubMed: 64477]

Kritzer MF, Goldman-Rakic PS. 1995; Intrinsic circuit organization of the major layers and sublayers of the dorsolateral prefrontal cortex in the rhesus monkey. J Comp Neurol. 359:131–143. [PubMed: 8557842]

Kuramoto E, Pan S, Furuta T, Tanaka YR, Iwai H, Yamanaka A, Ohno S, Kaneko T, Goto T, Hioki H. 2017; Individual mediodorsal thalamic neurons project to multiple areas of the rat prefrontal cortex: A single neuron-tracing study using virus vectors. J Comp Neurol. 525:166–185. [PubMed: 27275581]

Kuroda M, Murakami K, Oda S, Shinkai M, Kishi K. 1993; Direct synaptic connections between thalamocortical axon terminals from the mediodorsal thalamic nucleus (MD) and corticothalamic neurons to MD in the prefrontal cortex. Brain Res. 612:339–344. [PubMed: 7687193]

Lee S, Kruglikov I, Huang ZJ, Fishell G, Rudy B. 2013; A disinhibitory circuit mediates motor integration in the somatosensory cortex. Nat Neurosci. 16:1662–1670. [PubMed: 24097044]

Letzkus JJ, Wolff SB, Luthi A. 2015; Disinhibition, a Circuit Mechanism for Associative Learning and Memory. Neuron. 88:264–276. [PubMed: 26494276]

Letzkus JJ, Wolff SB, Meyer EM, Tovote P, Courtin J, Herry C, Luthi A. 2011; A disinhibitory microcircuit for associative fear learning in the auditory cortex. Nature. 480:331–335. [PubMed: 22158104]

LeVay S, Gilbert CD. 1976; Laminar patterns of geniculocortical projection in the cat. Brain Res. 113:1–19. [PubMed: 953720]

Li J, Guido W, Bickford ME. 2003; Two distinct types of corticothalamic EPSPs and their contribution to short-term synaptic plasticity. J Neurophysiol. 90:3429–3440. [PubMed: 12890796]

Li N, Daie K, Svoboda K, Druckmann S. 2016; Robust neuronal dynamics in premotor cortex during motor planning. Nature. 532:459–464. [PubMed: 27074502]

Little JP, Carter AG. 2012; Subcellular Synaptic Connectivity of Layer 2 Pyramidal Neurons in the Medial Prefrontal Cortex. J Neurosci. 32:12808–12819. [PubMed: 22973004]

Little JP, Carter aG. 2013; Synaptic Mechanisms Underlying Strong Reciprocal Connectivity between the Medial Prefrontal Cortex and Basolateral Amygdala. J Neurosci. 33:15333–15342. [PubMed: 24068800]

Llinás R, Jahnsen H. 1982; Electrophysiology of mammalian thalamic neurones in vitro. Nature. 297:406–408. [PubMed: 7078650]

Madisen L, Zwingman TA, Sunkin SM, Oh SW, Zariwala HA, Gu H, Ng LL, Palmiter RD, Hawrylycz MJ, Jones AR, et al. 2010; A robust and high-throughput Cre reporting and characterization system for the whole mouse brain. Nat Neurosci. 13:133–140. [PubMed: 20023653]

Mardinly AR, Oldenburg IA, Pégard NC, Sridharan S, Lyall E, Chesnov K, Brohawn SG, Waller L, Adesnik H. Precise multimodal optical control of neural ensemble activity. Nat Neurosci.

Mao T, Kusefoglu D, Hooks BM, Huber D, Petreanu L, Svoboda K. 2011; Long-range neuronal circuits underlying the interaction between sensory and motor cortex. Neuron. 72:111–123. [PubMed: 21982373]

Marin O. 2012; Interneuron dysfunction in psychiatric disorders. Nat Rev Neurosci. 13:107–120. [PubMed: 22251963]

Marlin JJ, Carter AG. 2014; GABA-A receptor inhibition of local calcium signaling in spines and dendrites. J Neurosci. 34:15898–15911. [PubMed: 25429132]

Miller EK, Cohen JD. 2001; An integrative theory of prefrontal cortex function. Annu Rev Neurosci. 24:167–202. [PubMed: 11283309]

Morishima M, Kawaguchi Y. 2006; Recurrent connection patterns of corticostriatal pyramidal cells in frontal cortex. J Neurosci. 26:4394–4405. [PubMed: 16624959]

Olsen SR, Bortone DS, Adesnik H, Scanziani M. 2012; Gain control by layer six in cortical circuits of vision. Nature. 483:47–U83. [PubMed: 22367547]

Parnaudeau S, O'Neill PK, Bolkan SS, Ward RD, Abbas AI, Roth BL, Balsam PD, Gordon JA, Kellendonk C. 2013; Inhibition of mediodorsal thalamus disrupts thalamofrontal connectivity and cognition. Neuron. 77:1151–1162. [PubMed: 23522049]

Petreanu L, Huber D, Sobczyk A, Svoboda K. 2007; Channelrhodopsin-2-assisted circuit mapping of long-range callosal projections. Nat Neurosci. 10:663–668. [PubMed: 17435752]

Petreanu L, Mao T, Sternson SM, Svoboda K. 2009; The subcellular organization of neocortical excitatory connections. Nature. 457:1142–1145. [PubMed: 19151697]

Pi HJ, Hangya B, Kvitsiani D, Sanders JI, Huang ZJ, Kepecs A. 2013; Cortical interneurons that specialize in disinhibitory control. Nature. 503:521–524. [PubMed: 24097352]

Pirot S, Jay TM, Glowinski J, Thierry AM. 1994; Anatomical and electrophysiological evidence for an excitatory amino acid pathway from the thalamic mediodorsal nucleus to the prefrontal cortex in the rat. Eur J Neurosci. 6:1225–1234. [PubMed: 7524967]

Reichova I, Sherman SM. 2004; Somatosensory corticothalamic projections: distinguishing drivers from modulators. J Neurophysiol. 92:2185–2197. [PubMed: 15140908]

Roth MM, Dahmen JC, Muir DR, Imhof F, Martini FJ, Hofer SB. 2016; Thalamic nuclei convey diverse contextual information to layer 1 of visual cortex. Nat Neurosci. 19:299–307. [PubMed: 26691828]

Saalmann YB. 2014; Intralaminar and medial thalamic influence on cortical synchrony, information transmission and cognition. Front Syst Neurosci. 8:83. [PubMed: 24847225]

Saalmann YB, Pinsk MA, Wang L, Li X, Kastner S. 2012; The pulvinar regulates information transmission between cortical areas based on attention demands. Science. 337:753–756. [PubMed: 22879517]

Schiller J, Schiller Y, Stuart G, Sakmann B. 1997; Calcium action potentials restricted to distal apical dendrites of rat neocortical pyramidal neurons. J Physiol. 505(Pt 3):605–616. [PubMed: 9457639]

Schmitt LI, Wimmer RD, Nakajima M, Happ M, Mofakham S, Halassa MM. 2017; Thalamic amplification of cortical connectivity sustains attentional control. Nature. 545:219–223. [PubMed: 28467827]

Sherman SM. 2016; Thalamus plays a central role in ongoing cortical functioning. Nat Neurosci. 19:533–541. [PubMed: 27021938]

Sherman SM, Guillery RW. 1998; On the actions that one nerve cell can have on another: distinguishing "drivers" from "modulators". Proc Natl Acad Sci U S A. 95:7121–7126. [PubMed: 9618549]

Spruston N. 2008; Pyramidal neurons: dendritic structure and synaptic integration. Nat Rev Neurosci. 9:206–221. [PubMed: 18270515]

Spruston N, Jaffe DB, Johnston D. 1994; Dendritic attenuation of synaptic potentials and currents: the role of passive membrane properties. Trends Neurosci. 17:161–166. [PubMed: 7517596]

Stratford KJ, Tarczy-Hornoch K, Martin KA, Bannister NJ, Jack JJ. 1996; Excitatory synaptic inputs to spiny stellate cells in cat visual cortex. Nature. 382:258–261. [PubMed: 8717041]

Stuart GJ, Häusser M. 2001; Dendritic coincidence detection of EPSPs and action potentials. Nat Neurosci. 4:63–71. [PubMed: 11135646]

Suter BA, Shepherd GM. 2015; Reciprocal interareal connections to corticospinal neurons in mouse M1 and S2. J Neurosci. 35:2959–2974. [PubMed: 25698734]

Takahashi N, Oertner TG, Hegemann P, Larkum ME. 2016; Active cortical dendrites modulate perception. Science. 354:1587–1590. [PubMed: 28008068]

Tervo DG, Hwang BY, Viswanathan S, Gaj T, Lavzin M, Ritola KD, Lindo S, Michael S, Kuleshova E, Ojala D, et al. 2016; A Designer AAV Variant Permits Efficient Retrograde Access to Projection Neurons. Neuron. 92:372–382. [PubMed: 27720486]

Theyel BB, Llano DA, Sherman SM. 2010; The corticothalamocortical circuit drives higher-order cortex in the mouse. Nat Neurosci. 13:84–88. [PubMed: 19966840]

Thomson AM, Bannister AP. 2003; Interlaminar connections in the neocortex. Cereb Cortex. 13:5–14. [PubMed: 12466210]

Uylings HB, Groenewegen HJ, Kolb B. 2003; Do rats have a prefrontal cortex? Behav Brain Res. 146:3–17. [PubMed: 14643455]

Van De Werd HJ, Rajkowska G, Evers P, Uylings HB. 2010; Cytoarchitectonic and chemoarchitectonic characterization of the prefrontal cortical areas in the mouse. Brain Struct Funct. 214:339–353. [PubMed: 20221886]

Vertes RP. 2001; Analysis of projections from the medial prefrontal cortex to the thalamus in the rat, with emphasis on nucleus reuniens. J Comp Neurol. 442:163–187.

Wang M, Ramos BP, Paspalas CD, Shu Y, Simen A, Duque A, Vijayraghavan S, Brennan A, Dudley A, Nou E, et al. 2007; Alpha2A-adrenoceptors strengthen working memory networks by inhibiting cAMP-HCN channel signaling in prefrontal cortex. Cell. 129:397–410. [PubMed: 17448997]

Wang XJ. 2001; Synaptic reverberation underlying mnemonic persistent activity. Trends Neurosci. 24:455–463. [PubMed: 11476885]

Wang XJ, Tegner J, Constantinidis C, Goldman-Rakic PS. 2004; Division of labor among distinct subtypes of inhibitory neurons in a cortical microcircuit of working memory. Proc Natl Acad Sci U S A. 101:1368–1373. [PubMed: 14742867]

White EL, Hersch SM. 1982; A quantitative study of thalamocortical and other synapses involving the apical dendrites of corticothalamic projection cells in mouse SmI cortex. J Neurocytol. 11:137–157. [PubMed: 6174701]

Wimmer RD, Schmitt LI, Davidson TJ, Nakajima M, Deisseroth K, Halassa MM. 2015; Thalamic control of sensory selection in divided attention. Nature. 526:705–709. [PubMed: 26503050]

Wise SP, Jones EG. 1976; The organization and postnatal development of the commissural projection of the rat somatic sensory cortex. J Comp Neurol. 168:313–343. [PubMed: 950383]

Xu W, Südhof TC. 2013; A neural circuit for memory specificity and generalization. Science. 339:1290–1295. [PubMed: 23493706]

Yamawaki N, Shepherd GMG. 2015; Synaptic circuit organization of motor corticothalamic neurons. J Neurosci. 35:2293–2307. [PubMed: 25653383]

Yizhar O, Fenno LE, Prigge M, Schneider F, Davidson TJ, O'Shea DJ, Sohal VS, Goshen I, Finkelstein J, Paz JT, et al. 2011; Neocortical excitation/inhibition balance in information processing and social dysfunction. Nature. 477:171–178. [PubMed: 21796121]

Zagha E, Casale AE, Sachdev RN, McGinley MJ, McCormick DA. 2013; Motor cortex feedback influences sensory processing by modulating network state. Neuron. 79:567–578. [PubMed: 23850595]

HIGHLIGHTS

- The PFC sends bifurcating projections to both MD and VM thalamus
- Cortical inputs from L5 and L6 differentially drive thalamo-cortical neurons
- MD and VM target distinct layers, cell types, and sub-cellular domains in the PFC
- Local PFC circuits connect thalamic inputs in L2/3 to cortico-thalamic outputs in L5

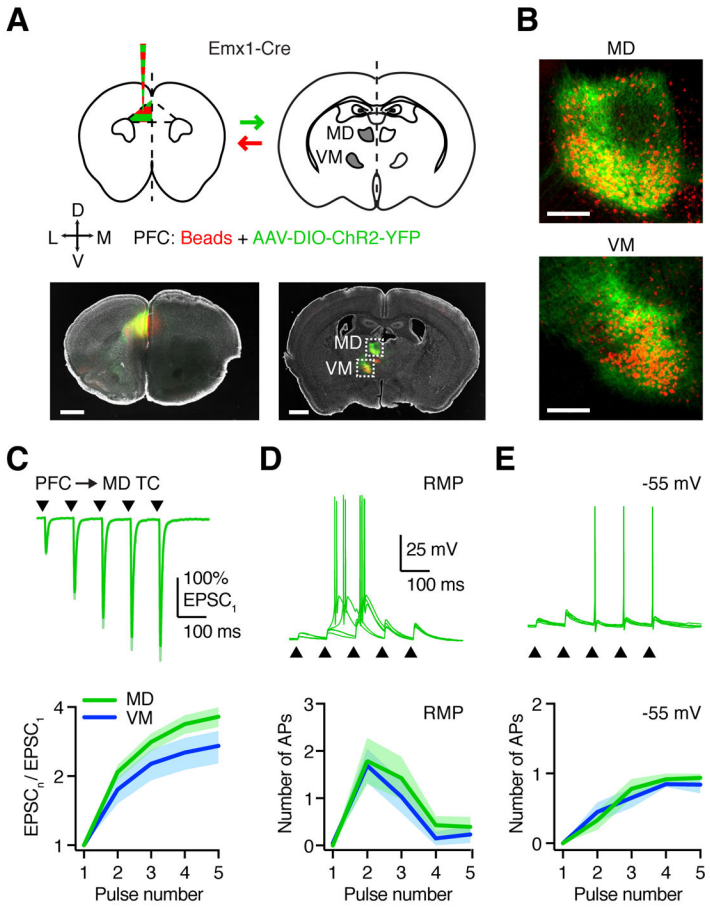

Figure 1. PFC drives reciprocally connected TC neurons in MD and VM

(A) Top: Injection schematic. AAV-DIO-ChR2-YFP and red retrobeads were co-injected into the prelimbic PFC of Emx1-Cre mice, followed by imaging in thalamic brain slices. Arrows indicate axon direction for projection-specific labeling. Bottom: Representative images showing injection site in PFC (left) and labeling in MD and VM thalamus (right). Grayscale images show DAPI labeling. Dashed boxes are insets shown in (B). Scale bars: 1000 μm.

(B) Retrograde cell (red) and anterograde axon (green) labeling in MD and VM thalamus. Scale bars: 200 μm.

(C) Top: PFC-evoked EPSCs at retrogradely labeled MD TC neurons, in response to 10 Hz LED stimulation trains (triangles) at −60 mV, following injections shown in (A). Traces are normalized to the amplitude of the first EPSC. Bottom: Summary of paired-pulse ratio (PPR) for PFC-evoked EPSCs at TC neurons in MD (green) and VM (blue) for each pulse (n) in the train.

(D) Top: PFC-evoked EPSPs and action potentials (APs) at retrogradely labeled MD TC neurons, in response to a similar train (triangles) at resting membrane potential (RMP), with five traces overlaid from the same cell. Bottom: Summary showing number of APs evoked at TC neurons for each pulse in the train.

(E) As in (D), for the same neurons held at −55 mV.

Values are mean ± SEM.

See also Figures S1 & S2

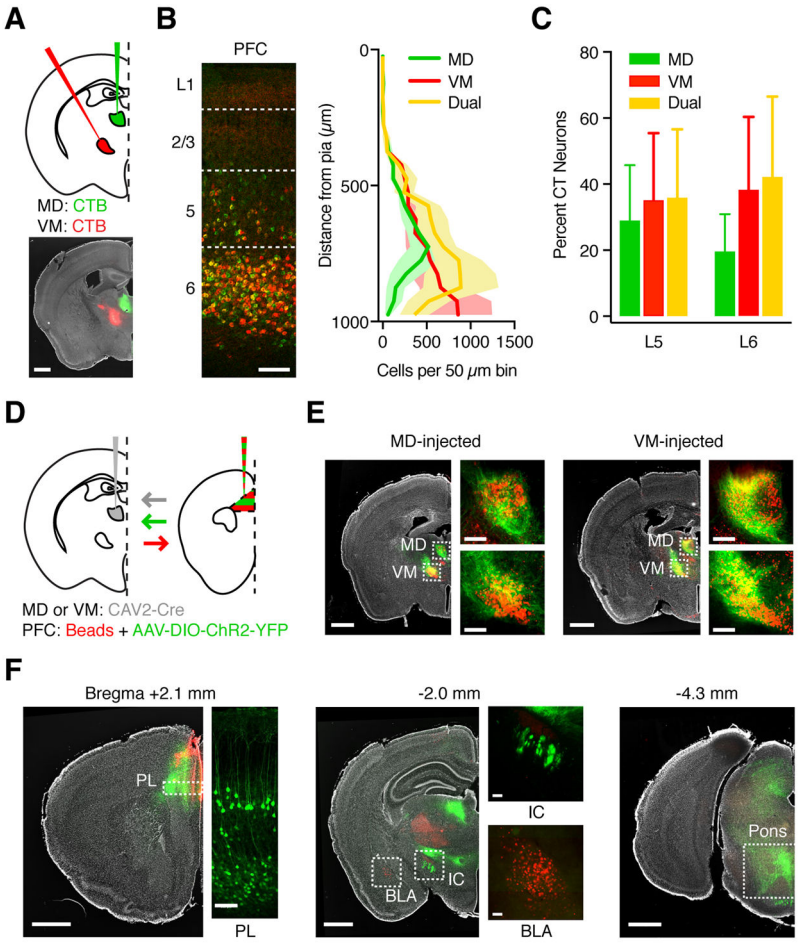

Figure 2. L5 and L6 CT neurons in PFC can project to both MD and VM

(A) Injection schematic and representative image. Retrogradely transported CTBs were injected into MD (green) and VM (red) of wild-type mice, followed by imaging in PFC. Grayscale image shows DAPI labeling. Scale bar: 1000 μm.

(B) Representative image (left) and quantification (right) of distribution of MD-projecting (green), VM-projecting (red), and dual-projecting (yellow) CT neurons across layers of prelimbic PFC. Image is from the same animal as in (A). Dashed lines: Layer boundaries. Scale bar: 100 μm.

(C) Summary of fraction of L5 and L6 CT neurons that project to MD, VM, or both nuclei.

(D) Injection schematic. Retrograde CAV2-Cre was injected into MD (as shown) or VM of wild-type mice, followed by anterograde AAV expressing Cre-dependent YFP and red retrobeads into PFC. Arrows indicate axon direction for projection-specific labeling.

(E) Representative images showing anterograde PFC axon (green) and retrogradely labeled TC neurons in the thalamus (red) from mice in which CAV2-Cre was injected in MD (left) or VM (right). Grayscale images show DAPI labeling. Dashed boxes are magnified in side images. Scale bars: 1000 μm or 200 μm.

(F) Representative images showing labeling of PFC neurons and projections following injections shown in (D). Left: Retrogradely labeled CT neurons in both L5 and L6 of prelimbic PFC (bregma +2.1 mm). Middle & right: CT axons in subcortical targets such as

the internal capsule (IC, bregma −2.0 mm) and pons (bregma −4.3 mm), but not BLA (bregma −2.0 mm). Scale bars: 1000 μm or 100 μm.

Values are mean ± SEM.

See also Figure S3

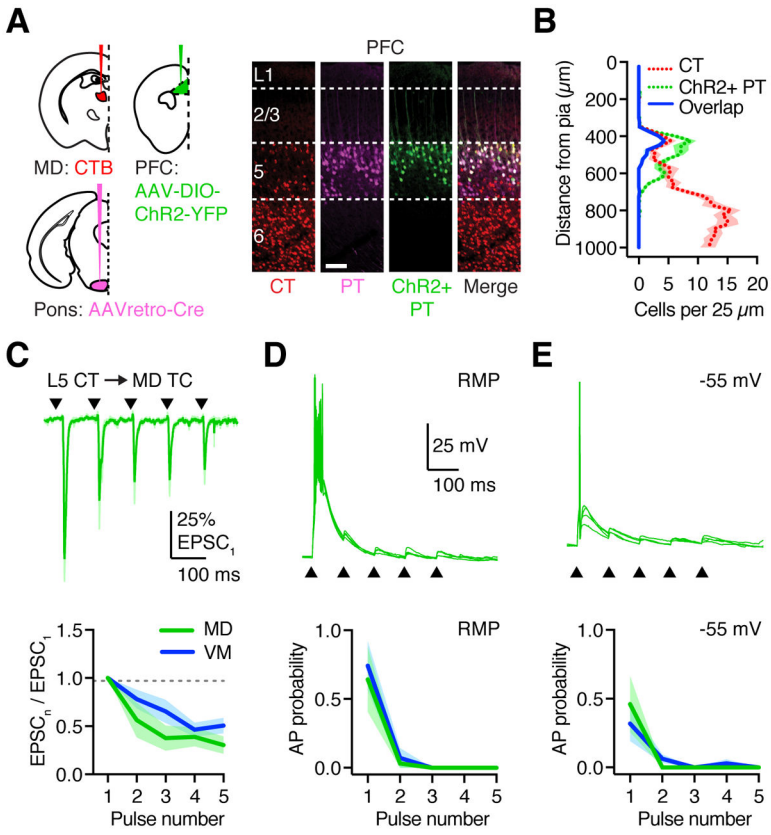

Figure 3. L5 CT inputs have distinct properties at TC neurons

(A) Injection schematic and representative images, with injection of CTB into MD (CT neurons), AAVretro-Cre-mCherry into the pons (Retro-Cre), and AAV-DIO-ChR2-YFP into the ipsilateral PFC (PT neurons). Scale bar: 100 μm.

(B) Summary distribution of retrogradely labeled CT neurons and AAVretro-Cre x AAV-DIO-ChR2-YFP co-infected PT neurons in PFC. Blue line indicates dual-labeled CT/PT neurons, which are largely restricted to superficial L5.

(C) Top: L5 CT-evoked EPSCs in retrogradely labeled MD TC neurons in response to 10 Hz LED stimulation trains (triangles) at −60 mV. Bottom: Summary of paired-pulse ratio (PPR) for L5 CT-evoked EPSCs at TC neurons in MD (green) and VM (blue) for each pulse (n) in the train.

(D) Top: L5 CT-evoked EPSPs and action potentials (APs) recorded from retrogradely labeled MD TC neurons in response to the train (triangles) at resting membrane potential (RMP), with four traces overlaid from the same cell. Bottom: Summary of AP probability evoked at TC neurons for each pulse in the train.

(E) As in (D), for the same neurons held at −55 mV.

Values are mean ± SEM.

See also Figure S3

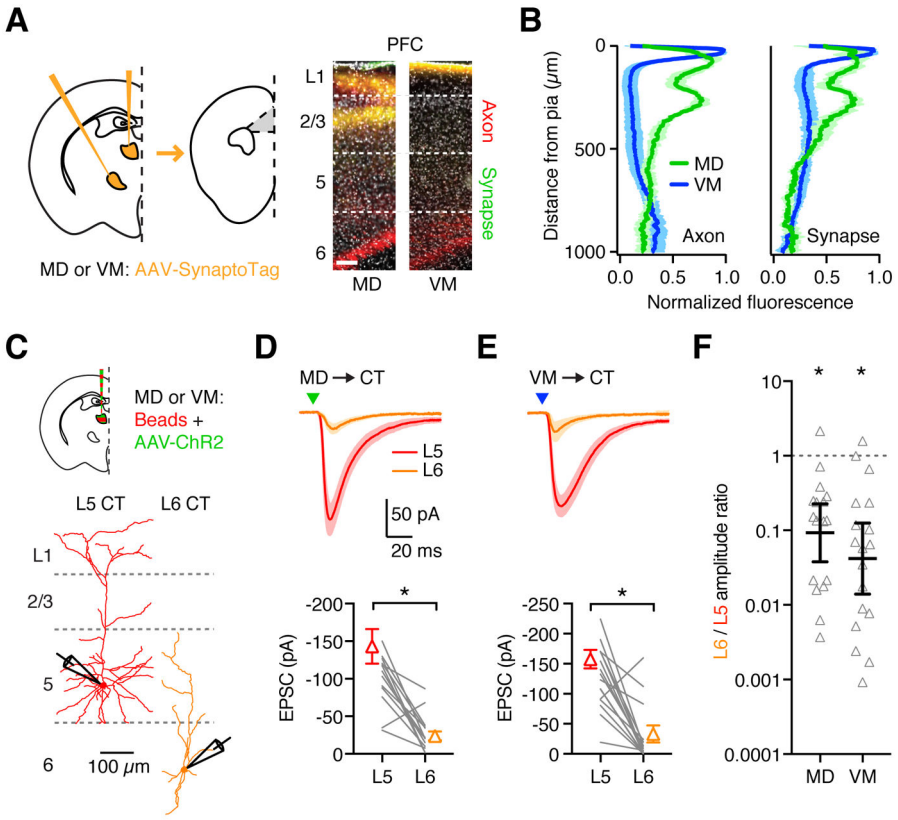

Figure 4. Thalamic inputs contact reciprocally connected CT neurons

(A) Left: Injection schematic, with AAV-SynaptoTag injected into MD or VM of wild-type mice, followed by imaging in PFC. Right: Representative images of prelimbic PFC, showing labeling of MD (left) and VM (right) axons (red) and synapses (green). Grayscale shows DAPI labeling. Scale bar: 100 μm.

(B) Summary of axon (left) and synapse (right) distribution from MD (green) and VM (blue) inputs to PFC.

(C) Top: Injection schematic. Bottom: Neuronal morphology and recording scheme. Recordings were made from pairs of retrogradely labeled L5 and L6 CT neurons during optogenetic activation of thalamic inputs.

(D) Top: MD-evoked EPSCs from paired L5 and L6 CT neurons in response to optogenetic stimulation (triangle) at −70 mV. Bottom: Summary of EPSC amplitudes in response to MD stimulation. Lines represent individual pairs.

(E) As in (D), for VM input.

(F) Summary of L6/L5 amplitude ratios for each recorded pair, calculated by dividing the L6 peak EPSC by the L5 peak EPSC. Note the logarithmic axis.

Values are mean ± SEM (B, D, E) or geometric mean ± 95% CI (F). * = $p < 0.05$

See also Figure S4 & S5

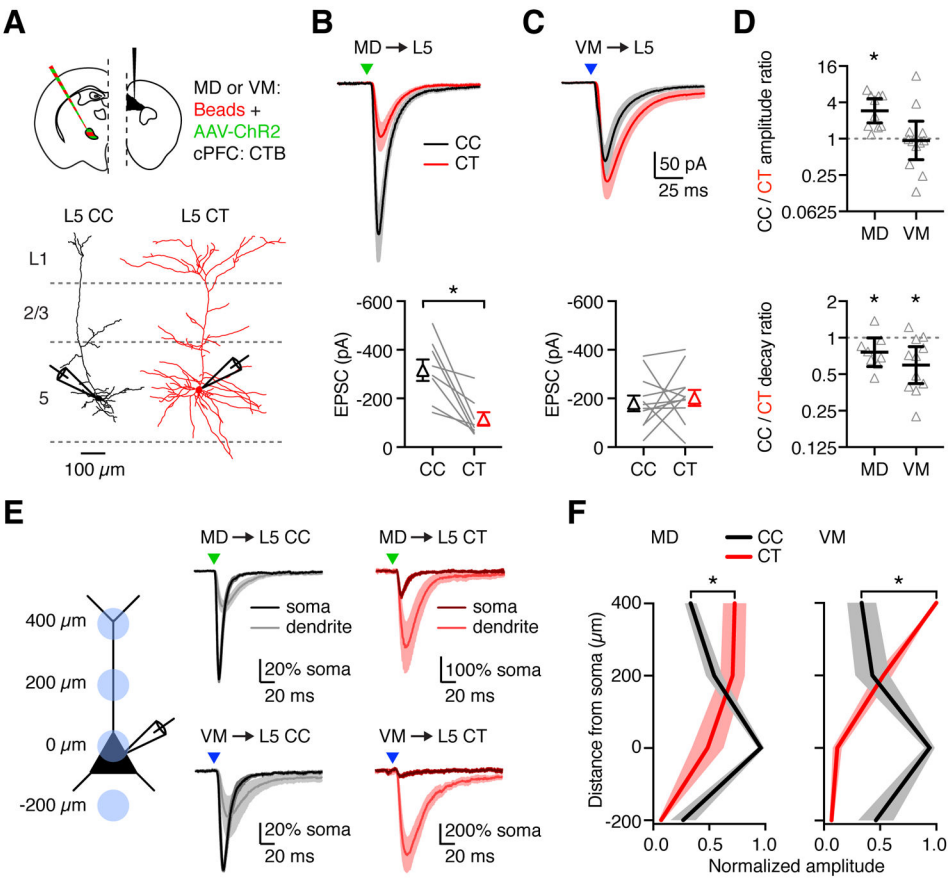

Figure 5. Differential targeting of MD and VM inputs onto L5 neurons

(A) Top: Injection schematic. Bottom: Neuronal morphology and recording scheme. Recordings were made from pairs of retrogradely labeled L5 CT and L5 CC neurons during optogenetic activation of thalamic inputs.

(B) Top: MD-evoked EPSCs from paired L5 CC (black) and L5 CT (red) neurons in response to optogenetic stimulation (triangle) at −70 mV. Bottom: Summary of EPSC amplitudes in response to MD stimulation. Lines represent individual pairs.

(C) As in (B), for VM input.

(D) Top: Summary of CC/CT amplitude ratios for each recorded pair, calculated by dividing the CC peak EPSC by the CT peak EPSC. Bottom: CC/CT decay ratios for the same pairs, calculated from the EPSC decay constants. Note the logarithmic axes.

(E) Left: Recording scheme for dendritic inputs. Recordings were made from L5 CC and L5 CT neurons with optogenetic stimulation at different locations along the dendrites. Distances shown are measured from the soma. Right: EPSCs evoked by subcellular activation (triangles) of MD (top) and VM (bottom) inputs onto L5 CC (black) and L5 CT (red) neurons. Traces represent mean EPSC ± SEM. EPSCs were normalized to the soma before averaging.

(F) Summary of EPSC amplitude in response to optogenetic stimulation of MD (left) or VM (right) inputs at different dendritic locations of L5 CC and L5 CT neurons. EPSC amplitudes were normalized to the largest response in each cell before averaging.

Values are mean ± SEM (B, C, F) or geometric mean ± 95% CI (D). * = $p < 0.05$
See also Figure S5

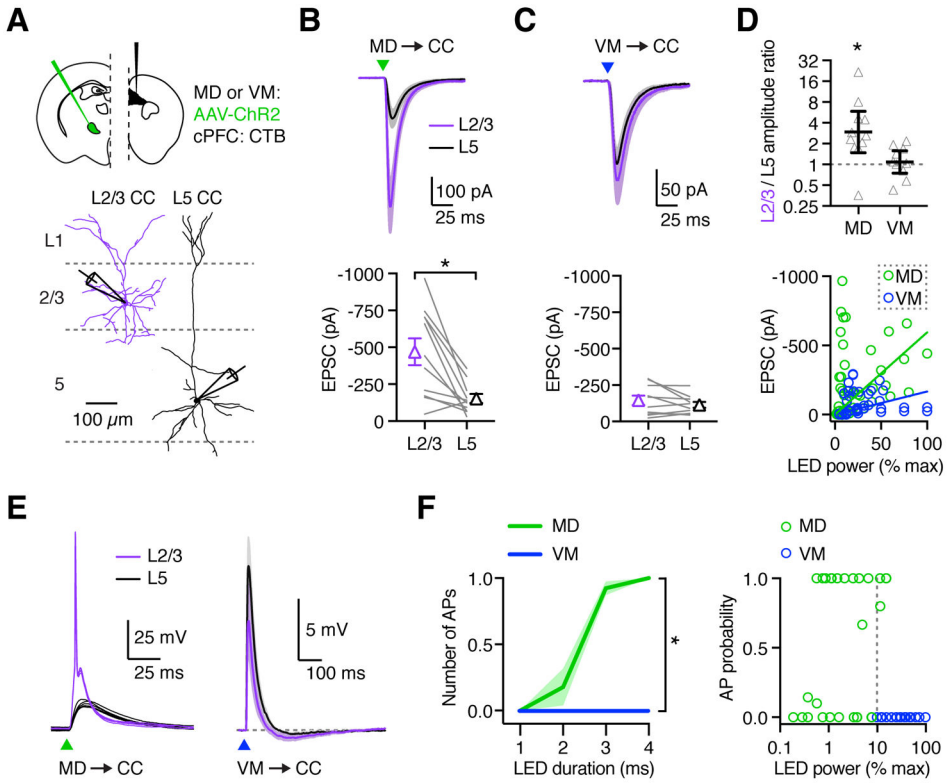

Figure 6. MD preferentially activates superficial CC neurons in PFC

(A) Top: Injection schematic. Bottom: Neuronal morphology and recording scheme. Recordings from pairs of retrogradely labeled L2/3 and L5 CC neurons during optogenetic activation of thalamic inputs.

(B) Top: MD-evoked EPSCs from paired L2/3 CC (purple) and L5 CC (black) neurons in response to optogenetic stimulation (triangle) at −70 mV. Bottom: Summary showing EPSC amplitudes in response to MD stimulation. Lines represent individual pairs.

(C) As in (B), for VM input.

(D) Top: Summary of L2/3/L5 amplitude ratios for each recorded pair, calculated by dividing the L2/3 peak EPSC by the L5 peak EPSC. Note the logarithmic axis. Bottom: Summary of MD- and VM-evoked (green and blue, respectively) EPSC amplitudes vs LED power, as a percentage of maximal power (9.8 mW). Solid lines represent linear regressions through the origin.

(E) EPSPs and action potentials (APs) from paired L2/3 CC (purple) and L5 CC (black) neurons in response to optogenetic stimulation (triangle) of MD (left) and VM (right) axons at RMP. MD example shows five traces from individual cells of the same pair. VM traces represent mean EPSPs averaged across all recorded neurons.

(F) Left: Summary of number of APs evoked from L2/3 CC neurons by MD and VM input across increasing LED pulse durations. Right: Summary of AP probability from L2/3 CC neurons in response to MD or VM input vs LED power, as a percentage of maximum power used (19.6 mW). Dashed line represents minimum LED power used for VM stimulation. Note the logarithmic axis.

Values are mean ± SEM (B, C, F) or geometric mean ± 95% CI (D). * = $p < 0.05$

See also Figure S5, S6, & S7

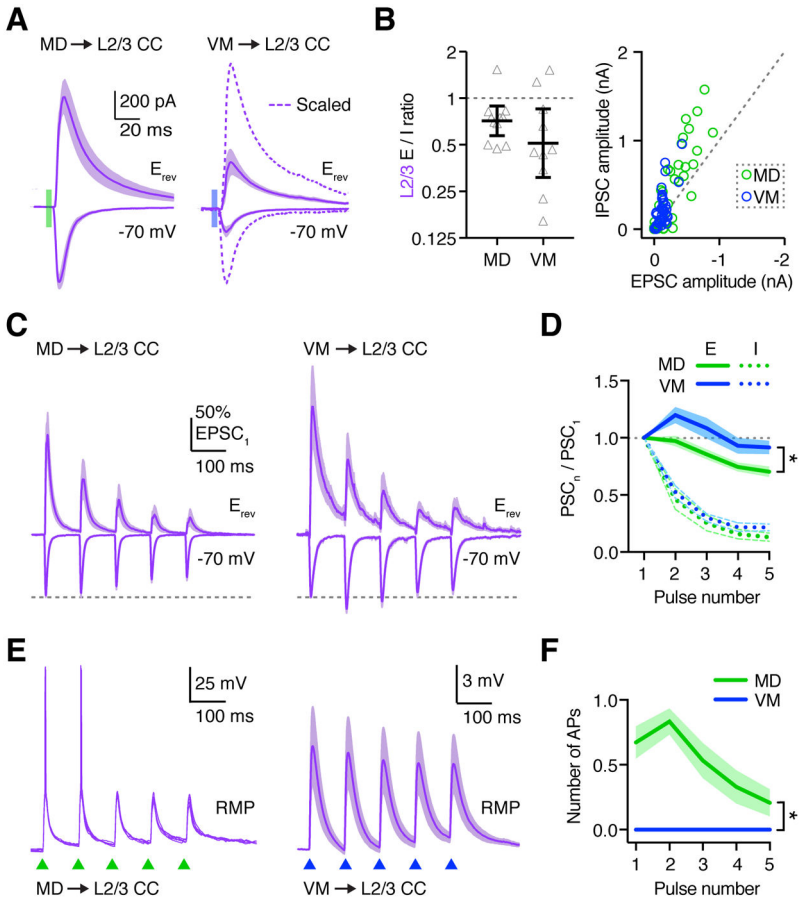

Figure 7. MD and VM inputs display distinct short-term dynamics

(A) EPSCs and IPSCs from L2/3 CC neurons in response to optogenetic stimulation of MD (left) or VM (right) inputs. Dashed line: Scaled to MD-evoked EPSC.

(B) Left: Summary of EPSC/IPSC (E/I) amplitude ratios for each recorded neuron, calculated by dividing the peak EPSC by the peak IPSC. Note the logarithmic axis. Right: Plot of EPSC amplitude vs IPSC amplitude for individual L2/3 neurons in response to optogenetic stimulation of MD or VM. Dashed line represents E/I = 1.

(C) Thalamus-evoked EPSCs at −70 mV and IPSCs at E_{rev} from L2/3 CC neurons, in response to 10 Hz LED stimulation trains (triangles) of MD (left) or VM (right) inputs. EPSCs and IPSCs are normalized to the first EPSC amplitude before averaging.

(D) Summary of paired-pulse ratio (PPR) for MD (green) and VM (inputs) for each pulse (n) in the train.

(E) Thalamus-evoked EPSPs and action potentials (APs) from L2/3 CC neurons, evoked by similar trains of MD (green triangles) or VM (blue triangles) inputs. Cells were recorded at RMP. MD example shows five traces from the same cell. VM traces represent mean EPSPs averaged across all recorded neurons.

(F) Summary of APs evoked by MD (green) or VM (blue) inputs at L2/3 CC neurons. Values are mean ± SEM (B, D, F). * = $p < 0.05$

See also Figure S7

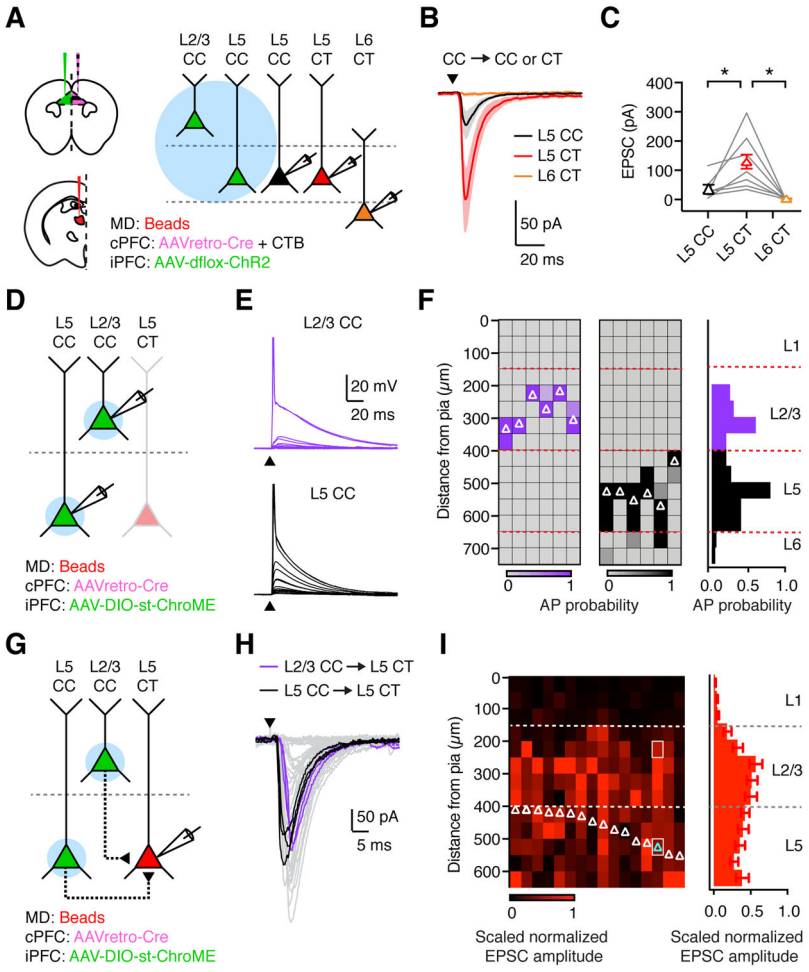

Figure 8. CC neurons in PFC preferentially contact L5 CT neurons

(A) Left: Injections of retrobeads in ipsilateral MD, AAVretro-Cre and CTB in contralateral PFC, and AAV-dflox-ChR2 in ipsilateral PFC. Right: recordings from retrogradely-labeled L5 CC, L5 CT, and L6 CT neurons during stimulation of local CC inputs.

(B) EPSCs recorded at −70 mV from triplets of L5 CC (black), L5 CT (red), and L6 CT (orange) neurons in response to optogenetic stimulation of local CC neurons.

(C) Summary of EPSC amplitudes, where lines represent individual triplets.

(D) Following similar injections to (A), but expressing st-ChroME in the ipsilateral PFC, recordings were made from pairs of st-ChroME-infected L2/3 and L5 CC neurons.

(E) Light-evoked depolarizations and action potentials (APs) from paired st-ChroME-expressing L2/3 CC (purple, top) and L5 CC (black, bottom) neurons, showing response to stimulation at different locations from the pia (0–700 μm, at 50 μm increments). Y–axis truncated to better highlight subthreshold responses.

(F) Left: Light-evoked AP probability for pairs of st-ChroME-expressing L2/3 (purple) and L5 (black) CC neurons at varying distances from pia. Each column is an individual cell, with recordings ordered pairwise from left to right. Soma locations of recorded neurons are indicated by white triangles. Right: Summary of AP probability versus distance from pia.

(G) Following similar injections to (D), recordings were made from L5 CT neurons.

(H) CC-evoked EPSCs from L5 CT neuron, showing responses from multiple trials recorded from a single cell, cyan triangle in (I), after stimulation at different locations from the pia. L2/3 (purple) and L5 (black) responses are highlighted, corresponding to white boxes in (I).
(I) Left: CC-evoked EPSCs from L5 CT neurons at varying distances from pia. Each column is a recorded neuron whose soma is indicated by a triangle. Responses are peak-normalized within each neuron and scaled to account for differences in AP probability in L2/3 and L5 CC neurons. Right: Summary of scaled peak-normalized EPSC amplitude at varying distances from pia.
Values are mean ± SEM (C, F, I). * = $p < 0.05$
See also Figure S8